CORE
Metadata, citation and similar papers at core.ac.uk
Provided by NASA Technical Reports Server

Four Decades of Space-Borne Radio Sounding

Robert F. Benson

Abstract

A review is given of the 38 rocket, satellite, and planetary payloads dedicated to ionospheric/magnetospheric radio sounding since 1961. Between 1961 and 1995, eleven sounding-rocket payloads from four countries evolved from proof-of-concept flights to sophisticated instruments. Some involved dual payloads, with the sounder transmitter on one and the sounder receiver on the other. The rocket sounders addressed specific space-plasma-wave questions, and provided improved measurements of ionospheric electron-density (N_e) field-aligned irregularities (FAI). Four countries launched 12 ionospheric topside-sounder satellites between 1962 and 1994, and an ionospheric sounder was placed on the Mir Space Station in 1998. Eleven magnetospheric radio sounders, most of the relaxation type, were launched from 1977 to 2000. The relaxation sounders used low-power transmitters, designed to stimulate plasma resonances for accurate local N_e determinations. The latest magnetospheric sounder designed for remote sensing incorporated long antennas and digital signal processing techniques to overcome the challenges posed by low N_e values and large propagation distances. Three radio sounders from three countries were included on payloads to extraterrestrial destinations from 1990 to 2003. The scientific accomplishments of space-borne radio sounders included (1) a wealth of global N_e information on the topside ionosphere and magnetosphere, based on vertical and magnetic-field-aligned N_e profiles; (2) accurate *in-situ* N_e values, even under low-density conditions; and (3) fundamental advances in our understanding of the excitation and propagation of plasma waves, which have even led to the prediction of a new plasma-wave mode.

1. Introduction

Table 1 provides a summary of the 38 rocket, satellite, and planetary payloads from eight countries (US, Canada, France, USSR, Norway, Japan, Sweden, and Italy) dedicated to ionospheric, magnetospheric, and planetary radio sounding, launched between 1961 and 2003. It indicates that the first radio sounding in space was performed from a US rocket launched on June 24, 1961, following the successful US rocket antenna-deployment test of June 14, 1961. These two rockets were followed by a US rocket flight into a disturbed ionosphere on October 31, 1961.

The first ionospheric sounding from a satellite was from the Canadian-built and US-launched Alouette 1. It was launched on September 29, 1962. It also established another first: the first satellite to be launched from the Western Test Range in California. It was the first satellite in the highly successful International Satellites for Ionospheric Studies (ISIS) program. The program, which included an additional eight countries (Australia, Finland, France, India, Japan, New Zealand, Norway, and the UK), included six satellites. Five of these satellites contained topside sounders. Four of the sounding satellites were Canadian-built and US-launched, and contained swept-frequency sounders (Alouette 1 and 2 and ISIS 1 and 2). The other two satellites in the program were built by the US (Explorer 20 and Explorer 31). Explorer 20 contained a topside sounder that operated on six fixed frequencies. This mode of operation proved to be so valuable for the investigation of N_e gradients and plasma resonances that it was included in the design of the sounders on ISIS 1 and 2. Explorer 31, also known as Direct Measurements Explorer-A (DMEA), was launched piggyback with Alouette 2. This dual-satellite mission was known as ISIS X. Explorer 31 demonstrated the compatibility of radio-sounder operations and *in-situ* measurements. The last satellite in the ISIS program, ISIS 2, was a complex observatory that included the first two auroral imagers in orbit. It demonstrated the compatibility of such imaging from a spinning satellite containing long sounder antennas.

The USSR and Japan launched an additional seven topside sounding satellites (Cosmos 381, ISS A and B, Intercosmos 19, EXOS C, Cosmos 1809, CORONAS 1) between 1970 and 1994. Cosmos 381 followed the launch of Cosmos 318 in 1969 that failed due to a rocket problem. The Cosmos 381 sounder, which was a pulsed sounder

Robert Benson is with the Geospace Physics Laboratory (Code 673), NASA Goddard Space Flight Center, Greenbelt, Maryland 20771, USA; Tel: +1 (301) 286-4037; Fax: +1 (301) 286-1433; E-mail: robert.f.benson@nasa.gov.

This is an invited Review of *Radio Science* from Commission H.

Table 1. A summary of space-borne radio sounders.*

Date	Country	s/c	T	Freq	Dp (m)	P (W)	Sounder Experiment and Comments	Sample Results and Reference
06/14/61	US	r			75	no tx	Antenna deployment test from spinning s/c	Successful demonstration [1]
06/24/61	US	r	s	f	32	3	4.07 & 5.97 MHz, 22 pps, 1,060 km apogee	1st topside sounding, quiet [2]
10/31/61	US	r	s	f	32	3	4.07 MHz, 22 pps, 1,070 km apogee	t/s sounding of spread F [3]
09/29/62	Canada	s	s	s	23, 46	100	Alouette 1, (0.5-12) 63 pps, 1,000 km polar	1st Global $N_e(h)$ t/s profiles [4]
08/25/64	US	s	s	f	19, 37	45	Exp. XX, 6 freq (1.5 to 7.22), 3 dp at 60°	N_e & res at 800 km polar [5, 6]
11/29/65	Canada	s	s	s	23, 73	300	Al. 2, (0.1–14.5), 30 pps, 500-3,000 polar	Compare *in-situ* techniques [4]
01/30/69	Canada	s	s	f/s	19, 73	400	ISIS 1, (0.1-20), 30 pps, 550-3,500 polar	More high-alt sound., AKR [4]
10/06/70	France	r	r	s	4	low	EIDI 1, 1-11 MHz in 0.4 s, 500 pps	3 f_H res: 2 waves 1 kHz apart [7]
10/22/70	France	r	r	s	4	low	EIDI 2, 2nd of 3 rocket relax sounders	Results given for EIDI 1 & 3 [8]
12/20/70	USSR	s	s	f	18	100	Cosmos 381, 985-1023 km, 74° inclination	N_e irreg. related to obs. UV [9, 10]
04/01/71	Canada	s	s	f/s	19, 73	400	ISIS 2, (0.1-20), 45 pps, 1,400 km polar	Compatible/w imagers, etc. [4]
06/25/71	US	r	r	s	10	60	0.5-4.5 MHz in ~ 4 s, 50 pps, waveform tel	f_T res freq variation obs. [11]
01/13/72	Norway	r	r	s	5	low	Mother-Daughter, 1.1-9 MHz, 192 km apog	Res identified as cone res [12]
02/06/73	Norway	r	r	s	8	low	Mother-Daughter, 0.8-5 MHz, 260 km apog	Cone & other res observed [13]
02/17/73	France	r	r	s	4, 8	2	EIDI 3, 0.44-5.52 MHz in 4 s, 10 ms listen	N_e irreg from f_N res [14]
02/29/76	Japan	s	s	s	11, 37	n/a	Ionosphere Sounding Satellite (ISS)-A	One month lifetime
04/20/77	France	s	r	s	42	low	GEOS 1, 0.3-77 kHz in 256 300 Hz steps	Magnetospheric N_e, 5-7 R_E, [15]
10/22/77	France	s	r	s	215	low	ISEE 1 (mother) w/sounder & 2 (daughter)	Magnetospheric N_e [16]
02/16/78	Japan	s	s	s	11, 37	150	ISS B, (0.5-14.8), 9 & 64 pps, 972-1220 km	Global maps of foF_2 [17]
07/14/78	France	s	r	s	42	low	GEOS 2, 0.3-77 kHz in 256 300 Hz steps	Plasmapause N_e features [18]
09/16/78	Japan	s	r	s	73,102	300	EXOS B (Jikiken), (.02-3), 227-30051 km	Plasmapause N_e irreg. [19]
02/27/79	USSR	s	s	s	15, 50	300	Intercosmos 19, 0.3-15.9 MHz in 5.8 s	Sounder-accel. electrons [20]
02/14/84	Japan	s	s	s	40	300	EXOS C (Ohzora), (0.1-16.0), 354-865 km	Wave-mode conversion [21]
02/22/86	Fran/Swed	s	r	s	80	low	V4H on Viking, 8-500 kHz in 3 freq. bands	N_e, plasmasphere & polar cap [22]
12/18/86	USSR	s	s	s	15,50	300	Cosmos 1809, (0.3-15.95), 58.6 pps	Freq. of sound-acc electrons [23]
01/30/89	Canada	r	s	s	4.4, 5.5	2	OEDIPUS A, 0-5 MHz bi-static sounder	Guided Z-mode propagation [24]
02/22/89	Japan	s	s	s	60	600	EXOS D (Akebono) 0.3-11.0, 10500 km ap.	Magnetosph. ducted echoes [25]
10/06/90	US/France	p	r	s	72	low	URAP on Ulysses, (0-50 kHz)	N_e in Io plasma torus [26-28]
03/03/94	USSR	s	s	s	15	n/a	CORONAS 1, 500 km, 82.5° inclination	Upper-hybrid emission band [29]
11/07/95	Canada	r	s	s	4.4, 5.5	10	OEDIPUS C, 0.1-8 MHz bi-static sounder	*In-situ* Faraday-rotation [30]
10/15/97	US/France	p	r	s	20	low	RPWS on Cassini, 3.6-115.2 kHz in 90 steps	N_e in vicinity of Saturn [31]
08/__/98	USSR	s	s	s	n/a	n/a	Orbital Complex (OC) on Mir Space Station	Sounding below F peak [32]
03/25/00	US	s	s	s	500, 20	10	IMAGE/RPI, (.003-3 MHz), tuned tx ant.	2D F-A N_e structures [33, 34]
07&08/00	France	s	r	s	88	low	WHISPER on 4 Cluster s/c, 2-80 kHz	Multipoint magnetospheric N_e [35]
06/02/03	Italy/US	p	s	s	40	5	MARSIS on Mars Express	Radio sounding of Mars iono [36]

**The date is the month/day/year of launch; s/c indicates that the spacecraft was either a rocket (r), satellite (s), or space probe (including a satellite around another planet) (p); T indicates the type of sounding, i.e., either a low-power relaxation sounder (r) for resonances or long-range sounding (s); Freq indicates that the sounding was at one or more fixed frequencies (f) or was a swept-frequency sounder (s); Dp (m) indicates the tip-to-tip length of the sounder dipole antenna(s) in meters; P (W) indicates the estimated peak radiated pulse power in watts; n/a indicates that the information could not be located by the author.*

using 20 fixed frequencies, was noteworthy for at least two reasons. First, the sounder design team was awarded the silver medal of the Moscow Exhibition of National Achievements. Second, one member of the design team (A. I. Galkin) was the father of I. A. Galkin, who is a key member of the sounder on the IMAGE satellite known as the Radio Plasma Imager (RPI), to be discussed below. In 1998, the USSR placed a radio sounder on the Mir Space Station. It was the first ionospheric sounder to be placed in orbit near the altitude of the N_e maximum, h_{max}.

From 1970 to 1995, eight ionospheric-sounding rockets built by four countries (France, US, Norway, and Canada), including four dual payloads (two each from Norway and Canada) were launched to investigate wave propagation and plasma resonances. The two French

rocket sounders launched in October 1970 were the first to telemeter the sounder-receiver waveform to the ground for plasma-resonance investigations. The US rocket sounder launched in June 1971 also transmitted the sounder-receiver waveform to the ground. It was the first "smart" sounder, in that the mode of operation was changed when strong plasma resonances were encountered.

From 1977 to 2000, eleven magnetospheric sounders (on the GEOS 1, ISEE 1, GEOS 2, EXOS B, Viking, EXOS D, IMAGE, and four Cluster satellites) from four countries (France, Japan, Sweden, and the US) were placed into orbit. The first was of the relaxation type, i.e., low-power transmissions designed to stimulate local plasma resonances. It operated from the European GEOS 1. Since the intended geostationary orbit was not achieved, most local electron-density (N_e) measurements, as deduced from the sounder-stimulated plasma resonances, were made from radial distances between five and seven Earth radii (R_E). The last four were also relaxation sounders, designated as WHISPER (Waves of HIgh frequency and Sounder for Probing Electron density by Relaxation); an identical sounder was placed on each Cluster satellite. The first magnetospheric sounding (out to a radial distance of nearly $2R_E$) to stimulate the full spectrum of plasma resonances, including a class of resonances known as the Dn resonances that were prominently stimulated in the ionosphere by Alouette 2 and ISIS 1 at radial distances out to about $1.5R_E$, was from the Japanese EXOS D (Akebono). The first long-range magnetospheric sounding (out to a radial distance of $8R_E$), using a programmable instrument with digital signal processing, was performed by the US sounder RPI on the IMAGE satellite. It was capable of low-frequency operation because of 500-m tip-to-tip dipole antennas in the spin plane. As in the case of the ISIS-2 observatory, IMAGE/RPI demonstrated the compatibility of remote imaging from a spinning satellite containing long sounder antennas.

Three extraterrestrial sounders, based on cooperative agreements among the US, France, and Italy, were launched between 1990 and 2003. Two were of the relaxation type: the Unified Radio And Plasma-wave instrument (URAP) on the Ulysses spacecraft to Jupiter (encountering the Io plasma torus in February 1992), and the Radio and Plasma Wave Science (RPWS) investigation on the Cassini spacecraft to Saturn. The Mars Advanced Radar for Subsurface and Ionospheric Sounding (MARSIS) instrument performed the first planetary ionospheric sounding at Mars in June 2005 from the Italian/US Mars Express.

While the above discussion highlights the many firsts associated with space-borne sounders, it is important to note that there was a fundamental first associated with ground-based sounders, commonly referred to as ionosondes. As pointed out by Warren Flock [37],

> The ionosonde, developed in 1925-1926 and used for monitoring the ionosphere since, was the first practical radar system of significance to be put into service. Operating in the HF frequency range and developed some years prior to surveillance radars, before the term radar (for radio detection and ranging) was introduced, the ionosonde may not be thought of by some as a radar, but it clearly is a special-purpose radar system.

Descriptions of the operation of swept-frequency ionosondes, and the interpretations of their data records, called ionograms, have been given in numerous books and publications [38-45]. Modern ionosondes, in use worldwide, incorporate both enhanced remote-sensing capabilities and automatic-analysis techniques [46-51].

The material in Table 1 was based on a comprehensive review of the ISIS program [52], a more-recent review that includes sounders other than those from the ISIS program [53], and information collected by the author with the aid of colleagues. It includes representative references from the various space-borne sounders: see [54] for a thorough review with references covering the first two decades of Alouette-1, Explorer-20, Alouette-2, and Explorer-31 operations. The related discussion in the text is based on the author's involvement with radio-sounding research using data from sounders carried on the Alouette 1 and 2, ISIS 1 and 2, OEDIPUS C, Ulysses, and IMAGE spacecraft. The objectives, history, and principal achievements of the ISIS program were discussed in a special issue of the *Proceedings of the IEEE* on topside sounding and the ionosphere [55]. There has been a resurgence of interest in the analysis of the Alouette-2, ISIS-1 and ISIS-2 topside sounder data, following a data-rescue effort that produced digital ionograms from a subset of the original analog telemetry tapes – many that were not previously processed into 35-mm film ionograms [56]. OEDIPUS C (Observations of Electric-field Distributions in the Ionospheric Plasma – a Unique Strategy) established a new record length for the longest tether in space at the time (approximately 1.2 km), breaking the record set by its predecessor, OEDIPUS A. The tether was cut shortly after the dual rocket payload achieved apogee, in order to provide the setting for unique bistatic radio-sounding experiments. The addition of an active sounding mode to the URAP instrument on the interplanetary Ulysses probe was the result of leadership by the late R. G. Stone, as PI, after instrument selection. IMAGE/RPI employed the longest antenna elements ever deployed on a spinning spacecraft, namely, orthogonal 500 m tip-to-tip dipoles in the spin plane, and a 20 m tip-to-tip dipole along the spin axis. The former were later shortened (presumably by micrometeorite impacts), but did not prevent successful active soundings (see, e.g., Section 1.2 of [57]).

This paper is not intended to be a thorough review of space-borne radio sounding, as approximately 1,000 scientific papers have been written based on these sounders. Rather, the plan is to discuss space-borne radio sounding as the gold standard for *in-situ* and remote electron-density (N_e) determinations in Section 2. Fundamental plasma

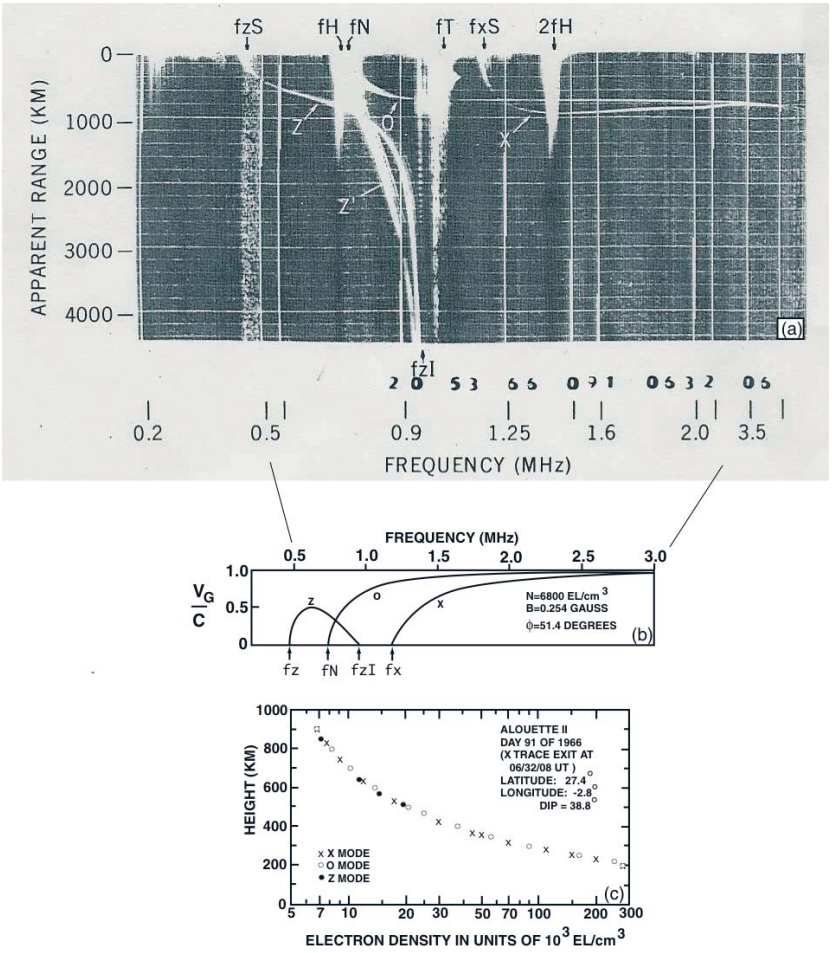

Figure 1. (a) An Alouette-2 mid-latitude ionogram, in negative format with signal reception in white on a black background, showing Z, O and X traces, plasma resonances, and a natural noise band (presumably in the Z mode): see the discussion in the text. (b) The group velocities corresponding to the plasma conditions at the satellite. (c) The calculated N_e values from each of the traces. (Figure adapted from [59, 60].)

processes, and gradients in N_e and the magnetic field, **B**, are discussed in Section 3. Enabling instrumental innovations are covered in Section 4. The importance of the antenna's orientation (relative to **B**) and of special plasma conditions for sounder-stimulated plasma phenomena are discussed in Sections 5 and 6, respectively. Nearly lossless propagation within N_e wave ducts are covered in Section 7. Section 8 provides a brief summary.

2. Space-Borne Radio Sounding as the Gold Standard for N_e Determinations

The original motivation for placing radio sounders in space was to obtain routine ionospheric N_e information over large geographic regions at altitudes above h_{max}, i.e., in the topside ionosphere: hence, the name ionospheric topside sounders. They are complementary to ground-based ionosondes, in that they provide orbit-plane topside N_e contours over a short time interval above a ground-based station where an ionosonde provided 24-hour coverage of the N_e profile below h_{max}. (Note: In each case, there are problems associated with the determination of h_{max}. Ionosonde measurements from the ground typically yield values that are about 10 km too low, and topside-sounder measurements from a satellite typically yield values that are about 10 km too high [58].) Since many of these topside-sounder satellites were in high-inclination orbits, the topside orbit-plane N_e contours corresponded to latitudinal contours. With an orbital period of about 90 minutes, these contours can be considered to be snapshots of the topside ionosphere covering about 40° of latitude in 10 minutes.

In addition to the differences in spatial and temporal coverage between ionosondes and topside sounders, there are fundamental differences in the received signals. These signals are recorded on data records called ionograms, which display the apparent range to the reflection point as a function of sounding frequency. The apparent range, also called the virtual range, is defined as $ct/2$, where c is the vacuum speed of light, and t is the roundtrip travel time. The apparent range is greater than the true range because, in the frequency range of main interest, the waves travel with a group velocity, v_g, considerably less than c. An example of a topside ionogram is presented in Figure 1a. The values of v_g for each of the principal ionospheric reflection traces, corresponding to the plasma conditions at the satellite as determined from the resonances and cutoffs (see next paragraph) on the ionogram of Figure 1a, are presented in Figure 1b.

Topside ionograms, such as the one in Figure 1a, differ from ground-based ionograms in that:

1. The apparent ranges of the echoes are much greater (they are typically within 1,000 km on ground-based ionograms [42]).
2. The echo traces extend to zero range (they typically do not appear below 100 km range on ground-based ionograms [42]).

3. The Z-mode wave is directly observed (it is only detected after a coupling to the O-mode wave on ground-based ionograms [39]).

4. Prominent plasma resonances, appearing as stalactites hanging from the zero apparent-range baseline, are present (these signals are mainly attributed to the reception of short-range electrostatic-mode echoes, and thus are not observed by ground-based sounders, where the antenna is in the neutral atmosphere [61]).

5. The ionosphere often generates noise bands that are received over the entire listening range, such as the one with a low-frequency cutoff coinciding with fzS in Figure 1a.

6. The ionosphere provides shielding of manmade interference in the frequency region below the ionospheric penetration frequency, fxF2 [62], allowing low powers to be used in topside sounding (a few hundred watts, rather than several kW as used in ground-based sounding in the 1960s), even though the propagation distances are much greater.

7. In the frequency region above fxF2, surface reflections are often received that enable information to be deduced about the entire (topside and bottomside) $N_e(h)$ profile [63], as well as terrain information [64]. At Mars, the sounder has been used as a ground-penetrating radar in this frequency region [65].

The labels at the top of the ionograms in Figure 1a use notation common in ionospheric publications. The labels correspond to (with commonly used magnetospheric physics notations in parentheses) the electron cyclotron frequency, f_H (f_{ce}) and harmonics nf_H (nf_{ce}); the electron plasma frequency, f_N (f_{pe}); the upper-hybrid frequency, f_T (f_{uh}); the cutoff frequency of the free-space extraordinary (X) mode, f_XS (the "S" is used to designate the cutoff frequency at the satellite); and the cutoff frequency, f_ZS , of the slow branch of the X mode, called the Z mode. The cutoff frequency of the free-space ordinary (O) mode corresponds to f_N . These frequencies have been defined in many books and review articles, e.g., see Sections 2 of the reviews [66] and [67]. They are defined below in terms of how they can be used to determine $|\mathbf{B}|$ and N_e :

$$|\mathbf{B}|\ [\mathrm{nT}] \cong 35.7\left(nf_H[\mathrm{kHz}]\right)/n \text{ , where } n = 1, 2, 3, \ldots \quad (1)$$

$$N_e\ [\mathrm{cm}^{-3}] \cong \left(f_N[\mathrm{kHz}]\right)^2/80.6\,, \quad (2)$$

$$f_N = \left(f_T^2 - f_H^2\right)^{1/2}, \quad (3)$$

$$f_N = \left[f_X\left(f_X - f_H\right)\right]^{1/2}, \quad (4)$$

$$f_N = \left[f_Z\left(f_Z + f_H\right)\right]^{1/2}. \quad (5)$$

Equations (4) and (5) lead to the useful expression

$$f_H = f_X - f_Z\,. \quad (6)$$

The quantity f_H (and hence $|\mathbf{B}|$ from Equation (1)) can often be determined to an accuracy of a few tenths of a percent, since there are typically more nf_H resonances present on an ionogram than in the example of Figure 1a, and the individual frequencies can typically be determined to an accuracy of a few percent or better (see, e.g., Appendix A of [56]). Once f_H is accurately determined, Equations (3) to (5) provide three independent measurements of f_N (and hence, N_e from Equation (2)), based on the observed values of f_T , f_X , and f_Z . Thus, together with the observed value for the f_N resonance and Equation (2), there are four independent determinations of N_e available from an ionogram such as the one shown in Figure 1a. Even when X and Z traces are not present, other resonances are often present to enable a spectral classification so as to determine N_e values to a precision of ~1%, even when $N_e \sim 1\ \mathrm{cm}^{-3}$ (see Section 3, and Section 3 of [68]).

The above redundancy in the determination of f_N , the typical accuracy of a few percent or better in determining the frequencies, and the minimal effect of spacecraft/plasma interactions on the determined values (see Section 3), leads to the concept of the space-borne sounder as the gold standard for the accurate determination of N_e . Indeed, the comparison of different DMEA probe techniques used the nearby Alouette-2 topside-sounder as the N_e reference level [69, 70]. Also, a comparison of data acquired from the DMEA and Alouette-2 cylindrical electrostatic probes indicated "no inherent incompatibility" between sounder and probe operations [71]. More recently, interleaved active and passive Radio Plasma Imager observations were used to confirm that accurate magnetospheric N_e measurements – i.e., within a few percent – can be deduced from the spectral features of the upper-hybrid emission band, which is often present on magnetospheric dynamic spectrograms [72]. On the other hand, in the ionosphere earlier investigations based on comparing passive wave observations and active sounder operations have shown that intense wave emissions seldom correspond to the upper-hybrid band, particularly to emissions at f_T (or f_{uh}) [29, 73]

However, the main objective of an ionospheric topside sounder is not to obtain accurate *in-situ* N_e values, but

to obtain complete vertical N_e profiles, $N_e(h)$, from the satellite altitude down to h_{max}. This information is obtained by inverting the following integral expression for the apparent range as a function of frequency, $P'(f)$, in order to obtain the electron-density distribution as a function of true altitude, i.e., $N_e(h)$:

$$P'(f) = \int n' dh \,, \qquad (7)$$

where $n' = n'\{N_e(h), f, |\mathbf{B}|(h), \phi(h)\}$ is the group refractive index, ϕ is the angle between **B** and the direction of propagation, and the integration is from the satellite altitude down to the height of reflection for frequency *f*. Equation (7) and its solution have been discussed in many texts and papers. The approach commonly used in the ISIS program is that of Jackson [60, 74, 75]. The approach is to partition the total integration path in Equation (7) into a number of laminations equal to the number of points selected on the X-mode reflection trace. The values of $|\mathbf{B}|$ and ϕ at the top of each lamination interval, including the first one starting at the satellite altitude, are obtained from a magnetic-field model. the variation of $|\mathbf{B}|$ within a lamination is based on the inverse cube law.

While the observed nf_H plasma resonances are not used to improve on the model's f_H value, other resonances are used with this model value to obtain a better determination of $f_X S$ in situations when it is difficult to accurately measure (see Section 3 of Appendix B of [74]). In some cases, particularly when N_e at the satellite altitude is very low, this iteration technique fails to converge. A modified iteration method has been shown to converge in such cases [76]. Refinements to true-height inversion techniques have continued (see, e.g., [77, 78]), and programs have been developed for the automatic processing of topside digital ionograms [79-82], which have been recently produced for Alouette 2, ISIS 1, and ISIS 2 [56].

Since the expressions for n' in Equation (7) are different for the O and X modes, and since the X mode has two branches, corresponding to a fast wave (termed the X mode) and a slow wave (termed the Z mode), the three ionospheric reflection traces, i.e., the Z, O, and X traces in Figure 1a, yield three independent ways to determine the $N_e(h)$ profile. The results of applying the inversion analysis to these three reflection traces in Figure 1a are shown in Figure 1c. The good agreement among the calculated $N_e(h)$ profile values based on the observed $P'(f)$ values from the Z, O, and X reflection traces provides confidence that these traces were properly identified, and that the two main assumptions used in the analysis were satisfied, namely, that the propagation was vertical and that the ionosphere was horizontally stratified. Note that the points corresponding to the O and X modes extended all the way down to near h_{max}, i.e., the altitude of maximum N_e near 200 km, whereas the points corresponding to the Z mode extended only down to about 500 km. This limitation was caused by the restriction of the Z mode to frequencies less than $f_Z I$ (called "Z infinity") in Figure 1b. In Figure 1a, $f_Z I$ appears as a narrowband signal just beyond 0.9 MHz hanging from the top of the ionogram, and it coincides with the asymptotic Z trace at the bottom of the ionogram. $f_Z I$ varies between f_N and f_T, depending on the angle of propagation. In spite of this propagation limit for the Z-mode echoes, IMAGE/RPI Z-mode echoes have been used to determine accurate N_e profiles along **B** for thousands of kilometers *above* the IMAGE satellite, i.e., into regions of decreasing N_e, when IMAGE was in the inner plasmasphere and at moderate to low altitudes over the poles [83]. These Z-mode echoes are possible because the Z-mode cutoff frequency, f_Z, in Equation (5) can have a local minimum leading to a trapping region for Z-mode waves [84]. An inversion routine was developed to convert the IMAGE/RPI Z-mode echoes into field-aligned N_e profiles in the vicinity of the spacecraft [83]. It was shown that these profiles were in good agreement with model values based on a different inversion procedure [85] used on IMAGE/RPI X-mode echoes .

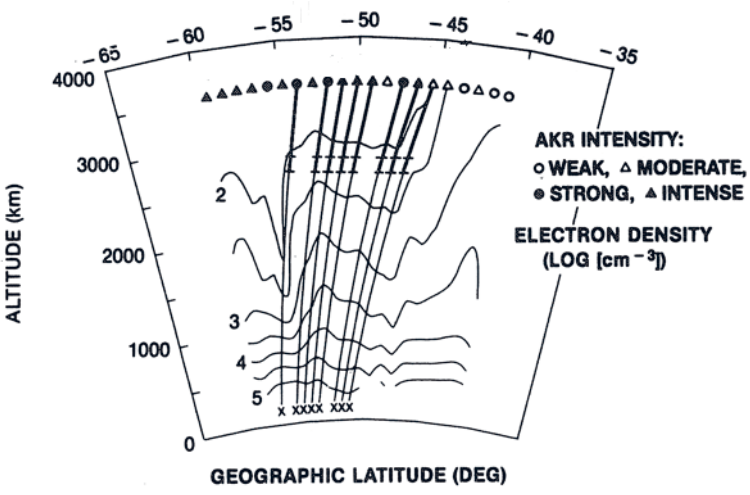

Figure 2. ISIS-1 sounder-derived N_e contours (10^2, 3×10^2, 10^3, etc.) and field-aligned projections through symbols indicating satellite position and auroral kilometric radiation intensity, with upper bold portions indicating the depth beneath the satellite of the auroral kilometric radiation source region (with estimated error limits), as determined from the spectral range of the auroral kilometric radiation (0959-1008 UT on 19 August 1969; adapted from [92]).

In addition to Z-, O-, and X-mode echoes, space-borne sounders have also detected echoes from waves propagating in the whistler (W) mode. Whistler-mode echoes were detected on high-latitude, early-morning Alouette-2 ionograms, and were attributed to ground reflections and a mode-coupling process in the lower ionosphere [86]. IMAGE/RPI commonly observed W- and Z-mode echoes when IMAGE was in the inner plasmasphere and at moderate to low altitudes over the polar regions [87]. Two types of W-mode echoes were observed by the Radio Plasma Imager: discrete and diffuse. The former were attributed to reflections from the bottom side of the ionosphere; the latter were attributed to scattering from field-aligned N_e irregularities (FAI) located within 2,000 km Earthward of the satellite, and near the magnetic field line passing through the satellite. These echoes were consistent with cross-**B** field-aligned irregularity scale sizes ranging from 10 m to 100 km. They support previous evidence [88] for the common occurrence of field-aligned irregularities in the topside ionosphere. Both types of W-mode echoes, and diffuse Z-mode echoes, have great potential for local and remote N_e diagnostics [87].

The results displayed in Figure 1c confirm the validity of the inversion procedure on a given ionogram with good traces. Furthermore, high-latitude conjunction studies between different topside-sounding satellites show good agreement among the $N_e(h)$ (field-aligned) profiles obtained from the different sounders [89]. However, accumulated evidence indicates that the topside Alouette-1 $N_e(h)$ profiles are too low, i.e., that they should be shifted upward parallel to the altitude axis [58]. This evidence included comparing simultaneous Alouette-1 topside profiles, ground-based incoherent scatter radar, and rocket measurements. It indicated that the profiles were about 20 km too low at altitudes below 600 km. Detailed topside-sounder/bottom-side-ionosonde comparisons, involving both Alouette-1 and Alouette-2 profiles, indicated that the topside altitude error was only a few percent of the propagation path. The differences were too large to be attributed to the vertical propagation assumption (rather than performing actual ray tracing). When the propagation path was short, i.e., corresponding to low satellite altitudes, a systematic error was detected in the range markers. An inspection of the ground reflection traces observed on Alouette-2 ionograms indicated that the best $N_e(h)$ profile results were obtained by assuming this systematic error to be 30 km, i.e., by reducing the virtual range by 30 km [58]. This range-marker problem led to the addition of a calibration range marker at 1667 km on the ISIS-2 topside sounder [90]. Later work, involving magnetic-field-aligned conjunction comparisons between low-altitude DE-2 *in-situ* Langmuir-probe measurements and ISIS-1 and -2 topside $N_e(h)$ profiles, indicated that the sounder-derived N_e values agreed with the probe measurements to within 30% near h_{max} on three of four comparisons. The agreement for the fourth comparison, in a region of N_e irregularities, was within 60% [91].

As stated by Jackson [58] concerning the errors discussed above, they "are usually too small to detract significantly from the general usefulness of topside ionograms." Many investigations have indicated this usefulness of the topside $N_e(h)$ profiles. For example, Alouette-2, ISIS-1, and ISIS-2 topside $N_e(h)$ profiles were used to reveal a tongue of F-region ionization (attributed to anti-sunward drift caused by magnetospheric convection) extending from the dayside across the polar cap during a magnetically-quiet day [89]. Topside ISIS-1 $N_e(h)$ profiles were combined to produce orbit-plane contours that together with simultaneous passive observations of the auroral kilometric radiation (AKR) frequency spectrum by the sounder receiver, determined the altitude extent of the auroral kilometric radiation source region below the satellite [92] (see Figure 2). Such orbit-plane N_e contours were compared with plasmapause magnetic-field lines (determined near the same time period by other satellites) to provide examples where the plasmapause projection occurred near the sharp low-latitude boundary of the nighttime ionospheric N_e main (mid-latitude) trough at high altitudes, but near the N_e minimum at lower altitudes. These contours were derived from ISIS-2 $N_e(h)$ hand-scaled profiles obtained from the National Space Science Data Center (NSSDC) ftp site. They may actually correspond to magnetic-field-aligned profiles, making the stated altitudes on the contours slightly low (see Figure 4 of [93]), but not impacting the conclusions of the study.

Large satellite topside sounding databases have enabled a number of diverse investigations. Alouette-1 and 2 hand-scaled $N_e(h)$ profiles have been used to create global-averaged $N_e(h)$ distributions [94]. Computer-scaled ISIS-2 digital ionograms produced $N_e(h)$ profiles that have been used to improve the International Reference Ionosphere (IRI) [95], and that have been used with IMAGE/RPI high-latitude magnetic-field-aligned magnetospheric N_e profiles to model the topside ionospheric F region and plasmasphere [96]. The International Reference Ionosphere is in particular need of improvement in the high-latitude topside ionosphere, as illustrated in Figure 10b of [56]. Global averaged F-region peak critical frequency (foF2) distributions obtained from the ISS-B topside sounder have been used to evaluate global foF2 models [97]. Regional averaged foF2 and h_{max} distributions obtained from the Intercosmos-19 topside sounder have been used to detect ionospheric signatures of tectonic activity [98], and for event studies, such as identifying ionospheric precursor signatures of large earthquakes, as reviewed in [53]. These are only a few examples of the scientific results that have come from the remote-sensing capabilities of space-borne radio sounders, particularly in the ability to derive topside $N_e(h)$ profiles. More examples can be found in a detailed review [54] of the results from the first two decades of the early satellites in the ISIS program.

The next sections will concentrate on some of the serendipitous scientific results that have resulted from these sounders, i.e., results not directly related to the main objective of obtaining vertical N_e profiles.

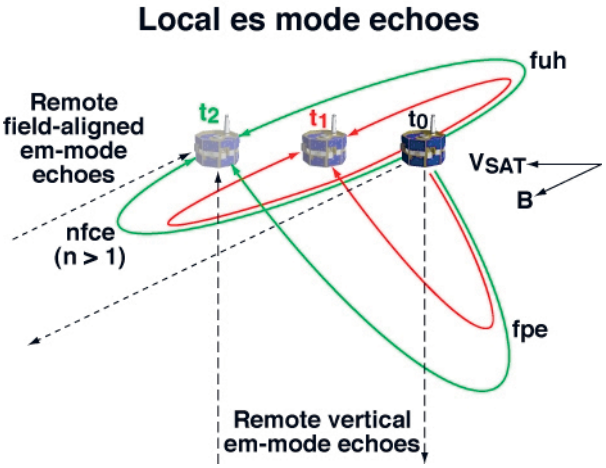

Figure 3. A schematic illustration of ray paths leading to echoes (at times t_1 and t_2) of sounder-generated (at time t_0) electrostatic (solid curves) and electromagnetic (dashed lines) waves [103].

3. Fundamental Plasma Processes, and Gradients in N_e and B

Spectacular signal returns on topside ionograms can often be explained using ray tracing, and special properties of the refractive index under certain plasma conditions, rather than invoking unusual N_e distributions. A classic example is the observation of a kink in the Z reflection trace that has been explained in terms of the peculiar properties of the Z-mode group refractive index when the wave frequency varies near f_{pe} [99]. Another is the concept of oblique echoes of sounder-generated electrostatic waves, due to the sensitivity of the refractive index to gradients in N_e and **B** near f_{pe}, f_{uh}, and nf_{ce}, to explain plasma resonances observed at these frequencies [100-102] (see Figure 3). Since these waves travel hundreds to thousands of meters into the medium, geophysical parameters deduced from the resonant frequencies using Equations (1) to (5) are not significantly affected by spacecraft/plasma interactions.

Note that the ray paths for the nf_{ce} resonances in Figure 3 exclude the case for $n = 1$. The parabolic nf_{ce} ray paths illustrated in Figure 3 correspond to electrostatic waves, with wave vectors, **k**, nearly perpendicular to **B**. The group velocities, $\mathbf{V}_s$, for these waves are approximately parallel to **B** when the wave frequency, *f*, is near nf_{ce}. Observational and theoretical investigations support the concept illustrated in Figure 3 for the resonances with $n > 1$. Additional effects may play a role in the case of $n = 2$, and the ray paths of the higher-order resonances in the topside ionosphere may be very short (see [104] and references therein). The nf_{ce} resonances stimulated by magnetospheric sounders are observed for much longer time durations [15]. The oblique-echo mechanism has yet to be applied to explain these observations. The nf_{ce} plasma wave dispersion curves with **k** approximately perpendicular to **B** are quite different for the case $n = 1$, however, and an interpretation of the observed features of the f_{ce} resonance has been sought for decades. A recent explanation for this resonance involves a solution to the hot-plasma dispersion equation with *f* near f_{ce} when **k** is approximately parallel to **B** [105]. It can explain the fringe pattern observed on the f_{ce} resonance during fixed-frequency operations in terms of the beating of two waves radiated from the plane containing the antenna and **B**. The waves in this interpretation are highly damped, which may explain the observed strong dependence of the duration of the f_{ce} resonance with altitude (longer duration under low-density conditions at high altitudes) in the Alouette-2 topside-sounder data [106].

There are two prominent sequences of resonances often observed between the nf_{ce} resonances that are not well explained by the oblique-echo mechanism. One is observed in the frequency region above f_{uh} [107], and the other is in the frequency region below f_{pe} [108], following the earlier discovery of the first member of the sequence [109]. The former are known as the Qn resonances, and have been explained in terms of a near matching of slowly-propagating electrostatic waves (known as Bernstein-mode waves) and the satellite velocity, $\mathbf{V}_s$ [110]. The latter are known as the Dn resonances, and have motivated five different theoretical interpretations (see the review in Section 1 of [111]). One proposed that the Dn resonances provided evidence for a new wave mode involving eigenmodes of cylindrical-electromagnetic plasma oscillations [112, 113] based on earlier theoretical predictions, involving force-free electromagnetic field (FFEMF) configurations, and that such oscillations would lead to a quantized emission spectrum with the frequencies of the different elements proportional to $\sqrt{n}$ [114, 115]. The cylindrical structures in this model correspond to the commonly observed field-aligned irregularity observed in space, not to the sheath surrounding the sounder antenna. The wave nature of these cylindrical oscillations was predicted as force-free electromagnetic field waves and solitons [116] that were later observed in a laboratory plasma [117]. The Dn resonances have prominent subsidiary resonances [108] that have been interpreted differently [118-120]. In the magnetosphere, the frequencies of the Qn resonances have been observed to deviate from the values expected for a Maxwellian electron velocity distribution [15, 68, 121, 122]. These observations have been investigated theoretically in two ways: (1) in terms of two Maxwellian components [121]; and (2) as a kappa distribution, where observations were shown to be consistent with a kappa value of two [123]. The Qn resonances also have subsidiary resonances [124, 125]. For a particular *n* value, the Qn resonance and its subsidiary have been attributed to the Doppler shifts of two waves, one propagating as a forward mode and the other as a backward mode, near but on both sides of the un-shifted Qn frequency [121]. The first member of each sequence is shown in Figure 4 [67]. This also shows one of the D1 subsidiary resonances (D1+); the hybrid relationship proposed to explain it [119]; and a resonance designated as "F" because it is often observed to float from the zero time-delay (or zero apparent range) baseline, and the approximate expression for its frequency [126].

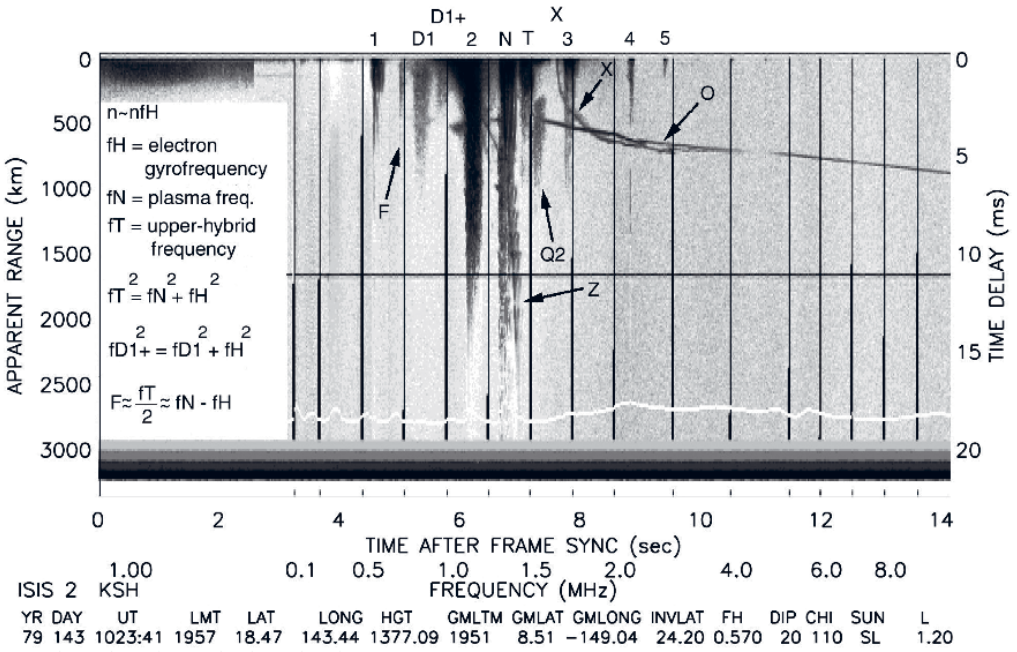

Figure 4. An ISIS-2 digital ionogram illustrating the D1, D1+, Q2, and F resonances (in addition to the resonances that can be explained by the oblique-echo mechanism characterized by Figure 3) [67].

The sequence nature of the Dn and Qn resonances is not apparent from a single ionogram, such as the one reproduced in Figure 4. However, as the plasma parameter, f_{pe}/f_{ce}, increases, higher members of the sequences appear. A presentation displaying the observed resonant frequencies from many ionograms, normalized by the observed f_{ce} versus the observed f_{pe}/f_{ce} illustrates the dominant control of the plasma parameter f_{pe}/f_{ce} in determining the frequency of these resonances [108, 118, 120, 125]. These resonances have proven to be of great value in the spectral classification of sounder-stimulated plasma resonances for the accurate determination of N_e, particularly in the magnetosphere, where clear X and Z traces are often not present [68]. While the Dn-sequence portion of this spectral classification is well explained by the cylindrical-electromagnetic plasma oscillations mechanism, some major issues remain. For example, these issues include deriving the fundamental D1 frequency from first principles (presently it is based on an empirical fit to the observations), and incorporating propagation aspects likely needed to explain the observed long time durations of the Dn resonances and the frequency splitting of the D1 resonance observed at mid latitudes [108, 127]. The issues also include explaining the abrupt disappearance of the $3f_{ce}$ resonance as the D2 resonance becomes prominent [125, 128] (see also Section 6), and investigating the role of sounder-stimulated ion motions leading to ion signatures on Dn resonances [128] (such ion signatures will be discussed in Sections 5 and 6). These issues, plus many other features of the Dn and Qn resonances, such as their excitation by natural process and (in the case of Dn) by rocket-borne electron guns, their use in determining N_e, and their relationship (in the case of Dn) to sounder-accelerated electrons, are discussed in Sections 1 and 3 of [111], Sections 3 of [68] and [113], and the "Discussion and Summary" of [129].

The revolutionary concept of interpreting the plasma resonances as oblique echoes, introduced by McAfee [100] after building on the work of Calvert [130] in interpreting the Z' echo (see, e.g., Figure 1a), was confirmed by innovative rocket experiments, as described in the next section.

4. Instrumental Innovation

Having had the privilege of working with Willi Hough on the ionosphere program, using the massive C3 ionosonde, during the first winter-over operation in 1957 at the Amundsen-Scott IGY South-Pole Station, under the leadership of Paul Siple [131], the author fully appreciates the degree of instrumental innovation involved in placing a swept-frequency ionospheric sounder on a satellite in 1962 [4, 55, 132, 133]. At the time, many thought that the Canadian-built Alouette-1 would at best have the then-typical satellite lifetime of a few months. The pessimism that the sounder would work was so strong that NASA had made no plans to use data from it. However, thanks to a *Robust Design* approach, the sounder provided a wealth of data for 10 years, even surviving higher-than-expected radiation from the unanticipated high-altitude hydrogen-bomb test over Johnston Island in the Pacific Ocean, seven weeks before the Alouette-1 launch [134, 135].

Several rocket payloads in the early 1970s were designed specifically to investigate the plasma resonances detected by ionospheric topside sounders. Rather than retrieving only the received pulse envelope, as in the case of the Alouette and ISIS topside sounders, these rocket-borne sounders telemetered the sounder-receiver waveform to the ground. Fourier analysis of this waveform resulted in unprecedented frequency accuracy. In one experiment,

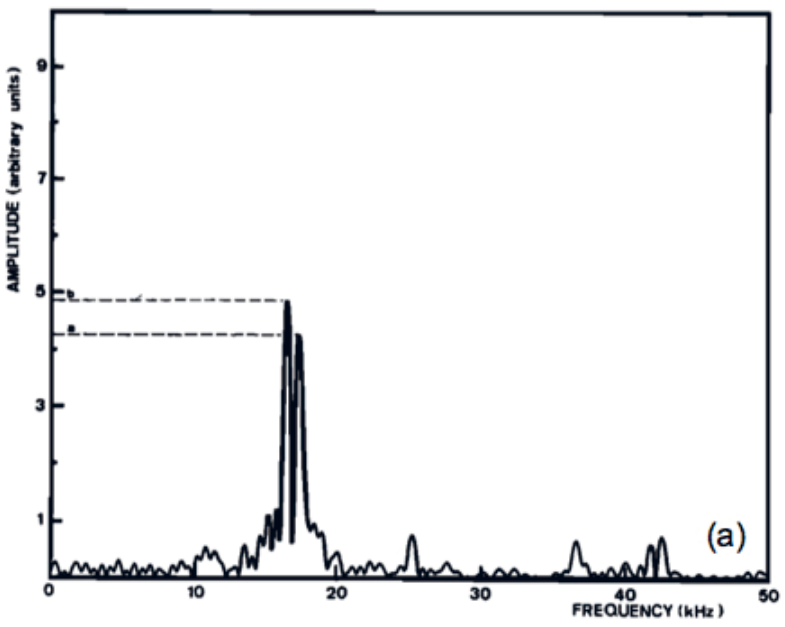

Figure 5a. The Fourier spectrum of the $3f_{ce}$ resonance waveform of the signal observed at 3.096 MHz when the rocket-borne sounder was at 480 km altitude, where $f_{pe} \cong 4.20$ MHz [7].

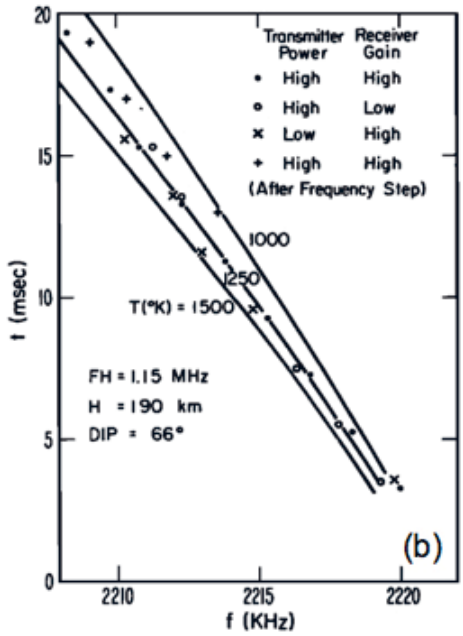

Figure 5b. The echo delay as a function of frequency for the f_{uh} resonance when f_{uh} was slightly less than $2f_{ce}$. The different symbols indicate different combinations of transmitter power and receiver gain during different modes of operation triggered by the large amplitude of the f_{uh} resonance, and the solid lines are theoretical predictions based on different electron temperatures [11].

the $3f_{ce}$ resonance was shown to be the result of a beating of two waves separated in frequency by about 1 kHz, as illustrated in Figure 5a [7]. These remarkable experimental-rocket results suggested that the $3f_{ce}$ resonance was the result of oblique echoes of electrostatic waves, i.e., the $3f_{ce}$ resonance was the result of a mechanism similar to the one proposed earlier for the f_{pe} and f_{uh} resonances [100, 101, 136]. In approximately the same timeframe as this rocket experiment, ray-tracing calculations demonstrated that an Alouette-2 $3f_{ce}$ resonance could be explained by the oblique-echo mechanism [102]. In another rocket experiment, the frequency variation of the received f_{uh} signal with delay time was measured, and found to agree with theoretical predictions based on oblique echoes of slowly propagating sounder-generated waves (see Figure 5b). Previous satellite ionospheric topside sounders could not observe this frequency variation with delay within the receiver bandwidth, because of onboard signal detection [11].

The highly successful bistatic rocket sounders OEDIPUS A and C obtained magnetic-field-aligned separations of the order of 1 km in the auroral topside ionosphere with the sounder transmitter on one payload and the sounder receiver on the other. OEDIPUS-C provided the first *in-situ* demonstration of Faraday rotation in space [30]. It also provided one of the first controlled quantitative confirmations of incoherent radiation theory in space, by detecting slow Z-mode radiation from sounder-accelerated electrons [137]. The OEDIPUS-C measurements of field-aligned irregularities, responsible for wave ducting of sounder generated X- and Z-mode waves, showed they consisted of N_e depletions of up to 21% with dimensions across **B** of a few kilometers [138].

The above rocket experiments introduced innovations in sounder design that made use of high data rates on short-duration missions dedicated to radio sounding. The design considerations for the sounder known as the Radio Plasma Imager (RPI) for the magnetospheric IMAGE satellite were quite different. IMAGE was a remote-sensing observatory with many instruments, and was far from being a dedicated sounding mission. The Radio Plasma Imager had to overcome programmatic challenges as well as instrumental challenges [139]. The instrumental challenges were many. Sounding was to be performed over great distances involving reflections from low-density plasmas, in spite of power, weight, and data-rate restrictions [66, 140]. The solution was to use 500 m tip-to-tip dipole antennas, transmit coded pulses that enabled signal processing to increase the signal-to-noise ratio so as to obtain long-range echoes with only 10 W radiated power, and to have a variety of programs and schedules to optimize the science return within the data restrictions [33]. The scientific results have been profound, as illustrated in a number of Radio Plasma Imager review papers [34, 141-143], reviews based on IMAGE/RPI and Cluster/WHISPER [144-147], and in other sections of this review.

Similarly, the design considerations for the WHISPER relaxation sounders on the magnetospheric Cluster satellites were also quite different. Here, the challenge was to deliver simultaneous N_e measurements on board the four spacecraft of the constellation in order to calculate instantaneous N_e spatial gradient vectors. The variability of plasma conditions near boundaries demanded a duration of each N_e

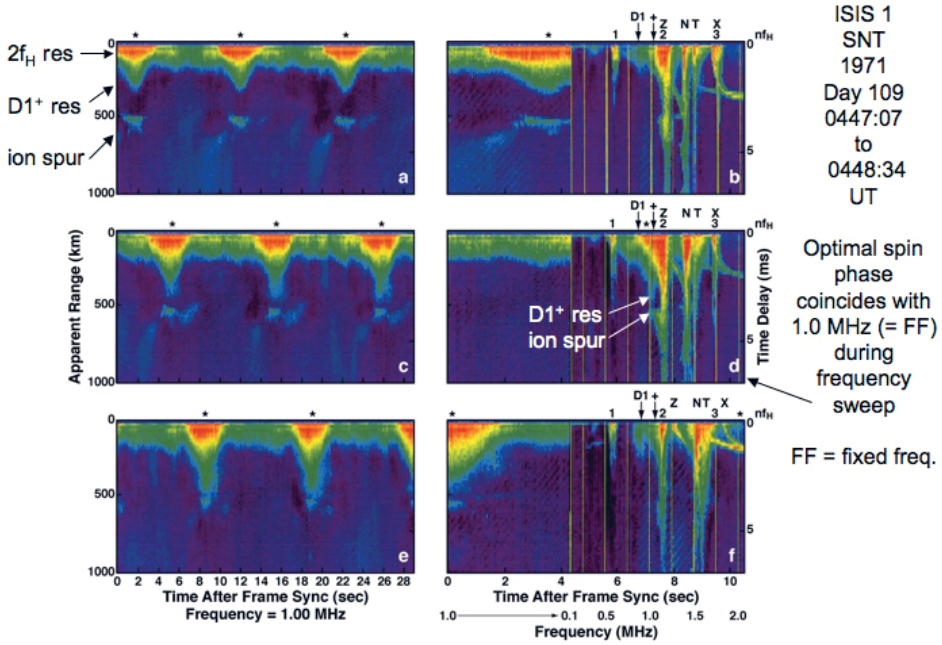

*Figure 6. Six consecutive ISIS-1 ionograms when the sounder was operating in the G mode (alternating between fixed-frequency and normal fixed/swept-frequency ionograms), illustrating the antenna spin modulation of the D1⁺ resonance, the $2f_H$ resonance, and its ion spur. The optimal spin phase for resonance excitation, the calculated value for the D1 resonance, and the calculated value for the D1⁺ resonance are designated at the top of each ionogram by *, D1, and +, respectively.*

determination significantly shorter than had been obtained on board previous magnetospheric sounders, like GEOS or ISEE. This requirement was met by implementing a fast Fourier transform, instead of a swept-frequency analyzer, in the receiver and analysis chain. The time resolution thus obtained (~ 1.5 s) allowed quasi-synchronization of the four independent measurements, via on-board UT clocks [35, 122, 148, 149].

5. Sounder-Stimulated Plasma Resonances: Importance of the Antenna's Orientation

There are several factors that can determine the occurrence of, and the characteristics of, sounder-stimulated plasma resonances, as have been discussed in a number of review papers [61, 102, 103, 150, 151]. Lockwood [152] was the first to show the importance of the antenna's orientation on the sounder excitation of plasma resonances. He showed that nf_{ce} resonances with high n were only observed by the Alouette-1 topside sounder when the relevant sounder antenna was nearly parallel to B. The relevant antenna was the one being used for transmission and reception. (In order to cover the wide frequency range, Alouette-1 employed crossed orthogonal dipoles of different lengths in the spin plane, with the longer dipole being used for transmission and reception at the lower frequencies, and the shorter dipole used for transmission and reception at the higher frequencies. The Alouette-2, ISIS-1, and ISIS-2 sounders operated in a similar manner [4].) While the effective radiated power does not appear to be a significant factor in determining the duration of the nf_{ce} resonances, as indicated by a comparison of selected Alouette-1 and Alouette-2 observations (see Section 5 of [106]), plasma conditions do play an important role. The following three studies indicated that for large f_{pe}/f_{ce}, plasma conditions may be the dominant factor:

1. An investigation of the time durations of Alouette-2 nf_{ce} resonances as a function of altitude near the dip equator found the greatest durations for resonances with $n > 5$ in the relatively dense plasma near perigee (see Figures 1 and 8b of [106]), where large values of f_{pe}/f_{ce} are expected.

2. An inspection of more than 200 Alouette-2 ionograms, selected so as to provide a wide range of f_{pe}/f_{ce} values within a narrow range of f_{ce} values, found few high-order nf_{ce} resonances excited when $f_{pe}/f_{ce} < 4$, but found the number of high-order harmonics to increase linearly with increasing f_{pe}/f_{ce} (see Figures 2, 21, and 22 of [125]).

3. A display of ionograms from two ISIS-1 passes, selected to obtain a range of f_{pe}/f_{ce} values from approximately one to 10, again while maintaining a narrow range of f_{ce} values, revealed a striking decrease in the duration and frequency width of the nf_{ce} resonances when $nf_{ce} > f_{uh}/f_{ce}$ (most apparent for $n > 2$). The greatest nf_{ce} resonant duration corresponded to the resonance with frequency closest to, but less than, f_{pe} [153]. Thus, these studies suggested that a particular antenna orientation is not required for the excitation of high-order nf_{ce} resonances when f_{pe}/f_{ce} is large (> 4). These results were consistent with the antenna-orientation restrictions for the detection of high-order nf_{ce} resonances found by Lockwood [152], since the Alouette-1 data set he used only sampled f_{pe}/f_{ce} values less than about four [125].

The sounder's antenna orientation plays an important role in determining the characteristics of the lower-order nf_{ce} resonances, but that role appears to be more complex than in the case of the high-order nf_{ce} resonances when f_{pe}/f_{ce} is small (< 4). An investigation of Explorer 20 fixed-frequency observations indicated that the $3f_{ce}$ resonance revealed a peak in duration with a pronounced fringe pattern when the antenna was perpendicular to **B,** but even stronger and longer-duration signals (without fringes) when it was parallel to **B** (see Figure 1b of [6]). The striking fringe pattern observed when the antenna was perpendicular to **B** is suggestive of two waves beating together, as observed for the $3f_{ce}$ resonance in a rocket experiment [7] as the antenna orientation relative to **B** varied approximately $\pm 20°$ around the perpendicular direction. The rocket observations were explained in terms of oblique echoes using analytic ray tracing [154]. This analytic ray-tracing approach was applied to Alouette-1 low-order nf_{ce} resonance observations, where it was found that near the magnetic equator, the maximum resonant duration would be expected when the antenna was nearly perpendicular to **B** (see Equation 31 of [104]). Low-latitude Alouette-1 observations indicated that strong plasma resonances at f_{pe} , f_{uh} , $2f_{ce}$, and $3f_{ce}$ could be observed using the long antenna when it was far from parallel to **B,** since high-order nf_{ce} resonances were observed a few seconds later on the short antenna [155] (an assumption supported by the plasma conditions, which corresponded to $f_{pe}/f_{ce} < 4$). ISIS-1 fixed-frequency observations of the f_{pe} resonance revealed strong maxima when the antenna was nearly perpendicular to **B** that were separated by a deep minimum when it was perpendicular to **B.** These observations have been explained by including the finite size of the antenna in the oblique-echo interpretation [156]. In general, it appears that plasma resonances at f_{pe} , f_{uh} , $2f_{ce}$, and $3f_{ce}$ can be stimulated over a wide range of antenna orientations. However, the signal strengths, time durations, and fringe patterns change in spectacular ways when the angle between the antenna and **B** is near either 0° or 90°.

Figure 6 presents six consecutive ISIS-1 ionograms, illustrating the enhancement of the $2f_{ce}$ resonance (the notation $2f_H$ is used in the figure) when the sounder antenna was in an optimal orientation. During this sequence, the ISIS-1 topside sounder alternated between fixed-frequency ionograms (Figures 6a, 6c, and 6e) and normal fixed/swept-frequency ionograms (expanded portions shown in Figures 6b, 6d, and 6f). From the later ionograms, it was clear that $f_{pe}/f_{ce} < 3$, and that the $2f_{ce}$ resonant frequency was significantly greater than 1.0 MHz, the frequency corresponding to the fixed-frequency operations. Note that even though the $2f_{ce}$ resonant frequency was greater than 1.0 MHz, the $2f_{ce}$ resonance was observed on the fixed-frequency ionograms (Figures 6a, 6c, and 6e) for a short duration with an intense (red) signal every time the sounder antenna was in an optimum orientation (these orientations are indicated by the * marks at the top of the ionograms). These short-duration intense signals resulted from a broadening of the bandwidth of the $2f_{ce}$ resonance during these favorable antenna orientations. (These signals shifted in phase from one fixed-frequency ionogram to the next fixed-frequency ionogram because the time interval between these ionograms was near but not an exact multiple of the antenna-spin period, the former being 57.9 s and the latter being about 20 s.) This broadening (to include 1.0 MHz) was seen on only one of the normal fixed/swept-frequency ionograms, namely, Figure 6d, the only ionogram where the sounder antenna was in an optimal orientation as the swept frequency was near 1.0 MHz (as indicated by the * in Figure 6d). In addition to the larger bandwidth, the intense (red) portion of the $2f_{ce}$ resonance was observed to have a longer duration on this ionogram than on Figures 6b and 6d. These characteristics suggested that the optimal antenna orientations, flagged by the * marks, corresponded to the antenna being nearly parallel to **B**, based on the Explorer-20 fixed-frequency observations where the strongest nf_{ce} resonances with no fringe patterns were observed under these conditions [6, 150].

There were two other striking features to notice in the expanded portion of the fixed/swept-frequency ionogram shown in Figure 6d, where this optimal antenna orientation occurred when the swept frequency was near 1.0 MHz. First, the $2f_{ce}$ resonance had an ion spur near 500 km apparent range that extended far enough on the low-frequency side of the resonance so as to reach the 1.0 MHz frequency marker. Second, there was a long-duration D1+ resonance near 1.0 MHz extending to nearly 500 km apparent range. Both of these features were only apparent on the fixed-frequency ionograms (Figures 6a, 6c, and 6e) under the * marks, indicating optimal antenna orientation, and they were less pronounced during the swept-frequency operation on Figures 6b and 6f, where the optimal antenna orientation (* marks) did not occur near the excitation of the $2f_{ce}$ resonance or the calculated positions of the D1+ resonances (indicated by the arrows below the + signs near 1.0 MHz). No theoretical explanation has been proposed to explain this dependence of the D1+ resonance stimulation on the antenna's orientation. However, this dependence was likely the reason the subsidiary Dn resonances were not always present with their corresponding main resonance on the same ionogram. The example in Figure 4, where the D1 and D1+ resonances were clearly seen on the same ionogram, is not typical.

The ion spur illustrated in Figure 6 (also known as a proton spur, because it appears after a time delay equal to the proton gyro period) clearly demonstrated that positive ion motions cannot be ignored if such sounder-stimulated phenomena are to be explained. These spurs were also apparent in the ionogram of Figure 4 near 500 and 1,000 km apparent range on the f_{pe} resonance (labeled "N"), and on the $2f_{ce}$ resonance (labeled "2"), where the spur extended nearly to the 1.0 MHz frequency marker at an apparent range slightly below the 500 km apparent-range label. Evidence for sounder-stimulated ion motions was first identified as a series of spurs on the sounder-generated plasma resonances on Alouette-1 topside ionograms [157]. These spurs have been

the subject of additional investigations using later topside sounders with better frequency resolution that identified specific resonances containing ion spurs [128, 158, 159]. Their explanation may be similar to the interpretation of the proton-cyclotron echoes observed on topside ionograms. These interpretations involve either proton bunching due to the RF-pulse-induced negative sounder-antenna potential [160, 161], or selective proton acceleration by the RF sounder pulse depending on the RF phase [162, 163]. Recent IMAGE/RPI observations at various altitudes within the plasmasphere have revealed intense W-mode proton-cyclotron echoes that were attributed to proton excitation as a transient event near the beginning of each RF sounder pulse. They were believed to be the most efficient at frequencies near and below the proton plasma frequency [57]. These Radio Plasma Imager observations also revealed two other forms of proton-cyclotron echoes that were similar to echoes observed by the Alouette/ISIS topside sounders. The first of these involved striking echoes at frequencies just above f_{ce} with a delay-time dependence on sounder frequency, suggesting warm-plasma propagation following a sounder-perturbed proton distribution possibly similar to that proposed for the ISIS observations [162]. The second involved proton-cyclotron echoes associated with the cold-plasma Z mode [57].

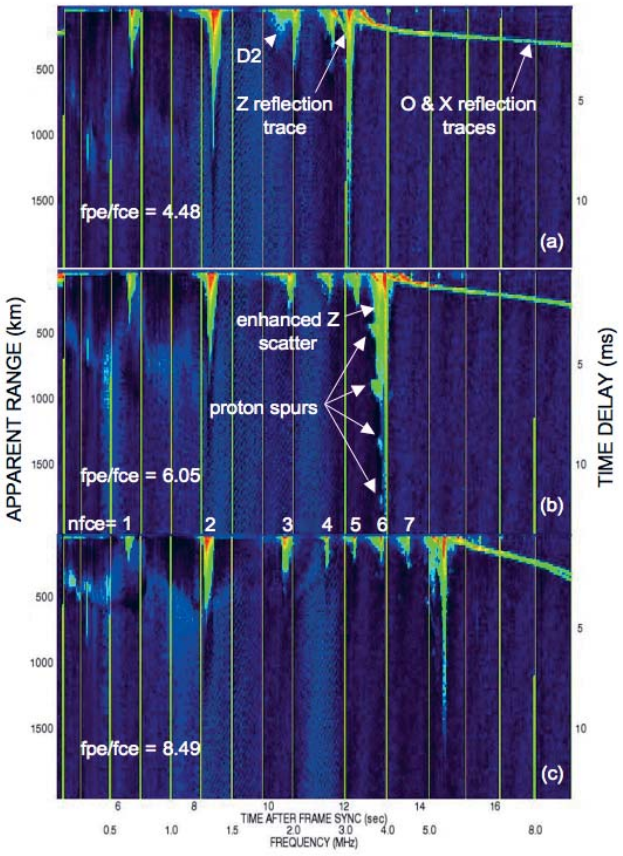

Figure 7. Portions of three consecutive ISIS-1 ionograms illustrating the changes in sounder-stimulated plasma phenomena as the ambient plasma conditions changed from $f_{pe}/f_{ce} < 5$ in (a) to $f_{pe}/f_{ce} > 8$ in (c). Spectacular enhancements occurred when $f_{pe}/f_{ce} \approx 6$ near 13 s after the frame sync, corresponding to a swept-frequency value of about 4.0 MHz in (b). (Recorded at QUI on 1971_006 with ISIS-1 at -11.9 GMLONG and 1914 GMLTM; 0037:36, 0038:06, and 0038:05 UT, 13.4, 11.5, 9.6 GMLAT, 704.5, 688.1, 673.3 km, in (a), (b), and (c), respectively; scaled f_{pe}/f_{ce} values: 3.03/0.676, 3.97/0.656, and 5.45/0.642 in (a), (b), and (c), respectively.)

6. Sounder-Stimulated Plasma Resonances: Importance of Special Plasma Conditions

Sounder-stimulated plasma phenomena have been observed to be particularly sensitive to the value of the plasma parameter f_{pe}/f_{ce}. There was a stepping through higher members of the Dn resonances as f_{pe}/f_{ce} increases [108, 118, 125]; an instability signature on the nf_{ce} resonances when $nf_{ce} < f_{uh}$ [153]; an enhancement of the proton spurs when $nf_{ce} \approx f_{pe}$ [128]; a strong diffuse resonance between f_{pe} and f_{uh} (known as DNT) that changed from a floating to a non-floating resonance as the plasma conditions changed from $f_{pe}/f_{ce} < 1$ to $f_{pe}/f_{ce} > 1$ [125]; an abrupt disappearance of the $3f_{ce}$ resonance when $f_{pe}/f_{ce} \approx 4$ (see Figure 9 of [128] and Figure 14 of [125]); and enhanced scattering of sounder-generated Z-mode waves when $f_{pe}/f_{ce} \approx n$ and $n \geq 4$, suggesting either sounder-enhanced or sounder-generated field-aligned irregularity [164]. Figure 7b illustrates this last phenomenon. Here, enhanced proton spurs and Z-mode scattered signals were observed when $f_{pe}/f_{ce} \approx 6$. During the three-ionogram sequence of Figure 7, f_{ce} decreased slightly from Figure 7a to 7c, and thus the frequencies of the nf_{ce} resonances varied only slightly from one ionogram to the next. Some of the more-prominent nf_{ce} resonances in Figure 7c are labeled at the top of the ionogram. However, the f_{pe} and f_{uh} resonances (coalescing into the long-duration signal between the Z and X reflection traces) increased considerably in frequency from one ionogram to the next. Only in Figure 7b, where the indicated signal enhancements were observed, was the ratio f_{pe}/f_{ce} near an integer value.

It has been shown that the enhanced signals attributed to wave scattering in Figure 7b were not due to more-efficient scattering when $f_{pe}/f_{ce} \approx n$ [165]. This result supports the argument that the wave scattering is from field-aligned irregularity stimulated, or enhanced, on a short time scale by the sounder [164]. These observations stimulated two theoretical studies:

1. An investigation of large-amplitude electron oscillations in cylindrical plasma structures aligned along **B**, i.e., with structures that could represent field-aligned irregularity, where enhanced resonance conditions were found when $f_{pe}/f_{ce} \approx n$ and where it was suggested that future work include dissipation and driver mechanisms [166].

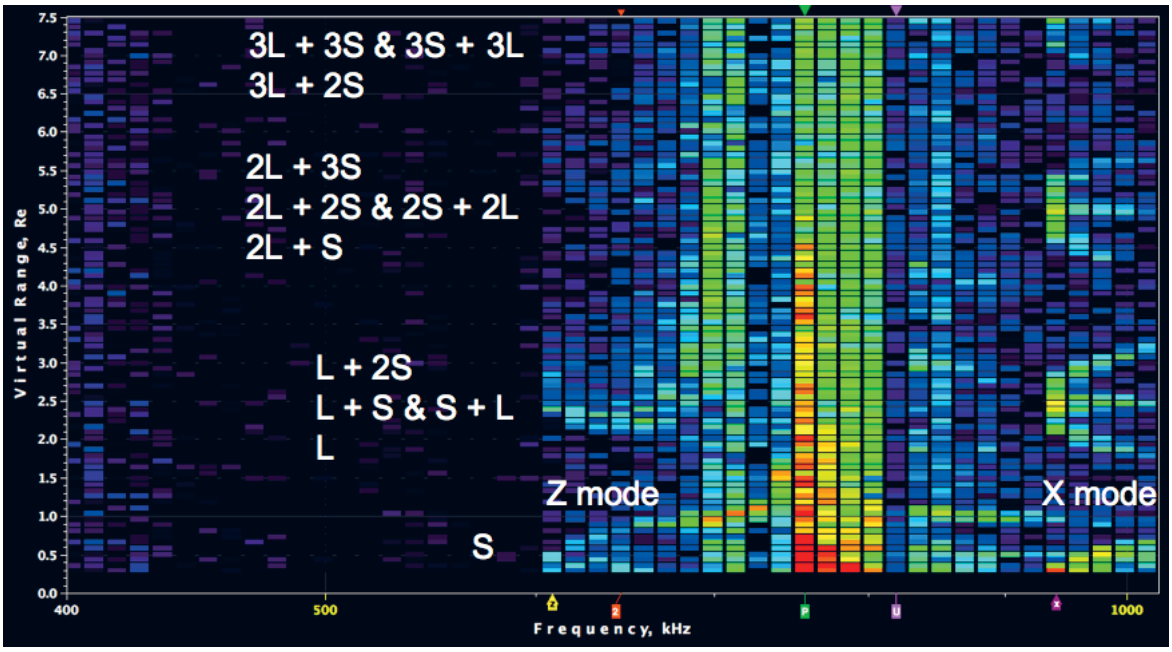

Figure 8. An IMAGE/RPI plasmagram (color-coded signal amplitude, with red most intense, displayed as virtual range from 0 to $7.5R_E$ on a linear scale as a function of sounding frequency from 400 to 1000 kHz on a logarithmic scale) with multiple Z- and X-mode epsilons, each containing traces due to multiple-hop hemisphere-to-hemisphere echoes. Echoes within the local hemisphere, i.e., the hemisphere containing the IMAGE satellite, are labeled "S" for short echo path, and echoes from the conjugate hemisphere are labeled "L" for long echo path. The outside labels on the bottom scale designate the Z- and X-mode cutoffs. The inner three labels on the bottom scale, and the three arrows at the top, identify the model value for $2f_{ce}$ and the calculated f_{pe} and f_{uh} values consistent with the observed wave cutoffs. (1850:28 UT on 31 August 2002; 11.1 MLAT, 0228 MLT, $1.5R_E$, $L = 1.57$.)

2. A four-wave coupling process, where a sounder-generated Z-mode wave acts as a pump wave at frequency f_O, which decays into two electron Bernstein waves and a purely growing meter-scale field-aligned irregularity when this Z-mode wave propagates to the O-mode reflection layer, where $f_O \approx f_{pe} \approx nf_{ce}$ [167]. In this latter study, the $f_{pe} \approx nf_{ce}$ condition would thus be achieved at some distance from the satellite, rather than at the satellite's location as observed.

A new resonance, stimulated by the Radio Plasma Imager on the IMAGE satellite, has been observed at a frequency about 15% above f_{ce} when the spacecraft is within the plasmasphere but at altitudes above about 7,000 km [57]. It was suggested that the lack of observation of this resonance by the Alouette-2 and ISIS-1 topside sounders may have been due to their relatively low apogees of 3,000 and 3,500 km, respectively [57]. Recall that in Section 3, it was pointed out that the there is both theoretical and observational evidence that the f_{ce} resonance itself is also expected to be observed in a stronger form in a rare rather than a dense plasma.

The plasma conditions encountered by the URAP relaxation sounder on Ulysses in Jupiter's Io plasma torus led to a spectrum of sounder-stimulated plasma resonances quite different from those encountered in the Earth's ionosphere or magnetosphere. The resonances were first interpreted in terms of the Dn resonances and the f_{pe} resonance, with no evidence for resonances at nf_{ce} or f_{uh}, to deduce both $|\mathbf{B}|$ and N_e along the spacecraft (s/c) trajectory [27, 168]. Later, they were interpreted as Doppler-shifted nf_{ce} resonances, due to the large (>100 km/s) spacecraft velocity relative to the co-rotating Jovian magnetospheric plasma, and were used to deduce both N_e and T_e along the spacecraft's trajectory [28]. These different interpretations generated some controversy [169-171].

7. Nearly Lossless Propagation within N_e Wave Ducts

The first satellite evidence of efficient propagation within N_e wave ducts was in the classic paper by Muldrew [172], published one year after the Alouette-1 launch. There have been many investigations of this non-vertical propagation [86] that include the concept of ducting within field-aligned irregularity in the whistler (W), Z, O, or X modes [83, 87, 173-176]. These ducted signals can take the shape of spectacular signals appearing as floating epsilons on ionospheric topside ionograms [177, 178] and on magnetospheric plasmagrams [83, 176, 179], as illustrated in Figure 8.

The intensities of the epsilon signatures, which are caused by multiple hemisphere-to-hemisphere echoes, suggest nearly lossless propagation within wave ducts. Such propagation has been well described for the W mode, as well as for the other modes (see, e.g., [173, 174]). Conjugate O-mode epsilons are not apparent in this figure, but when

they are observed, they provide an independent confirmation of field-aligned N_e profiles deduced from Radio Plasma Imager plasmagrams. This confirmation has indicated that what appears as an O-mode magnetospheric conjugate echo is the result of O-Z-O-wave-mode coupling [179], rather than direct O-mode ducting as proposed to explain the Alouette-1 conjugate echoes observed in the ionosphere [172]. The subject of O-Z mode coupling is also of great interest in ground-based wave-injection experiments (see, e.g., [180, 181]).

It is to be emphasized that the combination of echoes from the conjugate hemisphere with echoes from the local hemisphere enabled nearly instantaneous magnetic-field-aligned N_e profiles to be produced from one hemisphere to the other (with only the low-density region near the equator, where N_e is less than the value at the IMAGE satellite, being filled in by interpolation). As IMAGE travels along its orbit, consecutive hemisphere-to-hemisphere field-aligned profiles can be obtained for different radial distances, i.e., different L values. Such consecutive Radio Plasma Imager field-aligned N_e profiles have been combined to produce orbit-plane plasmaspheric N_e contours for a number of IMAGE orbits before, during, and after the large magnetic storm of March 31, 2001, in order to describe the plasmaspheric mass loss and refilling processes [182].

8. Summary

Space-borne radio sounding is a highly reliable technique, compatible with other instruments, for accurately measuring the local $|\mathbf{B}|$, and both local and remote N_e. Sounder observations have provided a wealth of information on the terrestrial topside ionosphere and magnetosphere, and on basic processes of wave generation and propagation. In spite of these great achievements – which have also been obtained in extraterrestrial plasmas – additional improvements to the International Reference Ionosphere for the topside ionosphere are required to meet the needs of present-day technological systems. Fundamental questions, such as the following, remain to be answered concerning many sounder-stimulated plasma phenomena:

1. What processes, in addition to the oblique-echo model, are needed to explain satellite observations of the $2f_{ce}$ resonances?
2. What is the cause of the abrupt disappearance of the $3f_{ce}$ resonance when $f_{pe}/f_{ce} \approx 4$?
3. Can the oblique-echo model explain the long durations observed for the magnetospheric nf_{ce} resonances?
4. What is the origin of the plasmaspheric resonance observed about 15% higher in frequency than f_{ce}, and the proton-cyclotron echoes observed both in a similar frequency region and near f_Z?
5. Will mechanisms applied to ionospheric and magnetospheric proton echoes be able to explain the proton spurs observed on sounder-stimulated plasma resonances, including their dependence on f_{pe}/f_{ce} and antenna orientation?
6. Can the fundamental D1 frequency be derived from first principles, can propagation aspects be incorporated into the cylindrical-electromagnetic plasma oscillations mechanism so as to explain the observed durations of the Dn resonances, and can the antenna spin-modulation dependence of the subsidiary Dn resonances be explained?
7. What causes the strong DNT resonance observed between f_{pe} and f_{uh} when f_{pe}/f_{ce} is near but less than one?
8. How does a space-borne sounder enhance, or generate, field-aligned irregularity when $f_{pe}/f_{ce} \approx n$ and $n \geq 4$?

9. Acknowledgements

The ISIS-1 ionograms in Figures 6 and 7 were located and retrieved using the NASA Goddard Space Flight Center (GSFC) Space Physics Data Facility (SPDF) CDAWeb service, available from the ISIS data-restoration project home page at http://nssdc.gsfc.nasa.gov/space/isis/isis-status.html. The Radio Plasma Imager plasmagram of Figure 8 was produced using the *BinBrowser* software, made available by the University of Massachusetts Lowell group under the leadership of B. W. Reinisch (see the IMAGE home page at http://image.gsfc.nasa.gov). Valuable comments and suggestions were received from D. L. Carpenter, I. A. Galkin, D. B. Muldrew, S. A. Pulinets, V. S. Sonwalkar, and two reviewers. Support for this work was provided in part by the NASA Living-With-a Star and Geospace programs and the GSFC Internal Research and Development (IRAD) program.

The Commission H Editor thanks the reviewers Pierrette Decreau and Gordon James for their assistance in evaluating this paper.

10. References

1. A. R. Molozzi and J. R. Richardson, "Measured Impedance of a Dipole Antenna in the Ionosphere," *Space Res.*, 7, 1967, pp. 489-505.

2. R. W. Knecht, T. E. V. Zandt, and S. Russell, "First Pulsed Radio Soundings of the Topside of the Ionosphere," *J. Geophys. Res.*, **66**, 1961, pp. 3078-3081.

3. R. W. Knecht and S. Russell, "Pulsed Radio Sounding of the Topside of the Ionosphere in the Presence of Spread F," *J. Geophys. Res.*, **67**, 1962, pp. 1178-1182.

4. C. A. Franklin and M. A. Maclean, "The Design of Swept-Frequency Topside Sounders," *Proc. IEEE*, **57**, 1969, pp. 897-929.

5. S. Russell and F. C. Zimmer, "Development of the Fixed-Frequency Topside-Sounder Satellite," *Proc. IEEE*, **57**, 1969, pp. 876-881.

6. W. Calvert and T. E. VanZandt, "Fixed-Frequency Observations of Plasma Resonances in the Topside Ionosphere," *J. Geophys. Res.*, **71**, 1966, pp. 1799-1813.

7. B. Higel, J. Bitoun, and M. Petit, "Rocket Observations of Two Waves Beating at 3fH Resonance," *J. Geophys. Res.*, **77**, 1972, pp. 6254-6258.

8. B. Higel and H. d. Feraudy, "Experimental and Theoretical First Approach to fH Plasma Resonance from a Relaxation Sounding Rocket Experiment," *Radio Sci.*, **12**, 1977, pp. 879-889.

9. G. V. Vasiliev, A. I. Galkin, V. E. Zasenko, A. S. Kasimanov, Y. V. Kushnerevski, et al., "Experiment on Pulse Radio Sounding of the Ionosphere above the Main Maximum of Ionization," Proceedings of the 10th All-Union Conference on Radiowave Propagation, Irkutsk, 26-30 July 1972, Moscow, Nauka, 1972, pp. 55-58 (in Russian).

10. G. V. Vasiliev, V. E. Zasenko, A. S. Kasimanov, S. M. Matyushonok, N. S. Mozerov, et al., Satellite Ionosonde IS-2," Proceedings of the 10th All-Union Conference on Radiowave Propagation, Irkutsk, 26-30 July 1972, Moscow, Nauka, 1972, pp. 59-61 (in Russian).

11. J. R. McAfee, T. L. Thompson, W. Calvert, and J. M. Warnock, "Rocket Observations of Topside Resonances," *J. Geophys. Res.*, 77, 28, 1972, pp. 5542-5550.

12. K. Folkestad and J. Troim, "A Resonance Phenomenon Observed in a Swept Frequency Experiment on a Mother-Daughter Ionospheric Rocket," *J. Atmos. Terr. Phys.*, **36**, 1974, pp. 667-685.

13. K. Folkestad, J. Troim, and J. Bording, "Interpretation of Signals Detected on a Mother-Daughter Rocket in the Polar F-Region," *J. Atmos. Terr. Phys.*, **38**, 1976, pp. 335-350.

14. B. Higel, "Small-Scale Irregularities of Electron Density in the F Region from f_N Resonances Observed by a Rocket-Borne Relaxation Sounding Experiment," *Radio Sci.*, **13**, 1978, pp. 901-916.

15. J. Etcheto and J. J. Bloch, "Plasma Density Measurements from the GEOS-1 Relaxation Sounder," *Space Science Reviews*, **22**, 1978, pp. 597-610.

16. C. C. Harvey, J. Etcheto, Y. D. Javel, R. Manning, and M. Petit, "The ISEE Electron Density Experiment," *IEEE Trans. Geosci. Electr.*, **GE-16**, 3, 1978, pp. 231-238.

17. T. Maruyama and N. Matuura, "Global Distribution of Occurrence Probability of Spread Echoes Based on ISS-B Observation," *J. Radio Res. Lab.*, **27**, 1980, pp. 201-216.

18. B. Higel and L. Wu, "Electron Density and Plasmapause Characteristics at 6.6 RE: A Statistical Study of the GEOS 2 Relaxation Sounder Data," *J. Geophys. Res.*, **89**, A3, 1984, pp. 1583-1601.

19. T. Ono and H. Oya, "Electrostatic Electron Cyclotron Harmonic (ESCH) Echoes Found near the Plasmapause by the EXOS-B (Jikiken) Satellite," *Geophys. Res. Lett.*, **15**, 1988, pp. 156-159.

20. Y. I. Galperin, R. Z. Sagdeev, F. K. Shuiskaya, Y. V. Lisakov, V. V. Migulin, et al., "Detection of Electron Acceleration in the Ionospheric Plasma under the Influence of High-Power Radio Radiation near the Local Plasma Frequency Aboard the Space Vehicle Interkosmos 19," *Cosmic Res.*, **19**, 1981, pp. 22-29.

21. H. Oya, A. Morioka, and T. Obara, "Leaked AKR and Terrestrial Hectometric Radiations Discovered by the Plasma Wave and Planetary Plasma Sounder Experiments on Board the Ohzora (EXOS-C) Satellite-Instrumentation and Observation Results of, Plasma Wave Phenomena," *J. Geomagn. Geoelectr.*, **37**, 1985, pp. 237-262.

22. P. M. E. Decreau, M. Hamlin, R. Massif, H. d. Feraudy, E. Pawela, et al., "Plasma Probing by Active Wave Experiments on the Viking Satellite," *Ann. Geophys.*, **5A**, 4, 1987, pp. 181-186.

23. F. K. Shuiskaya, Y. I. Galperin, A. A. Serov, N. V. Baranets, Y. V. Kushnerevsky, et al., "Resonant Heating of the Ionospheric Plasma by Powerful Radiopulses Aboard the Intercosmos-19 and Cosmos-1809 Satellites," *Planet. Space Sci.*, **38**, 1990, pp. 173-180.

24. H. G. James, "Guided Z Mode Propagation Observed in the OEDIPUS A Tethered Rocket Experiment," *J. Geophys. Res.*, **96**, 1991, pp. 17865-17878.

25. H. Oya, A. Morioka, K. Kobayashi, M. Iizima, T. Ono, et al., "Plasma Wave Observation and Sounder Experiments (PWS) Using the Akebono (EXOS-D) Satellite – Instrumentation and Initial Results Including Discovery of the High Altitude Equatorial Plasma Turbulence," *J. Geomagn. Geoelectr.*, **42**, 1990, pp. 411-442.

26. R. G. Stone et al., "Ulysses Radio and Plasma Wave Observations in the Jupiter Environment," *Science*, **257**, 1992, pp. 1524-1531.

27. V. A. Osherovich, R. F. Benson, J. Fainberg, R. G. Stone, and R. J. MacDowall, "Sounder Stimulated Dn Resonances in Jupiter's Io Plasma Torus," *J. Geophys. Res.*, **98**, 1993, pp. 18751-18756.

28. P. LeSager, P. Canu, and N. Cornilleau-Wehrlin, "Impact of the Ulysses Velocity on the Diagnosis of the Electron Density by the Unified Radio and Plasma Wave Sounder in the Outskirts of the Io Torus," *J. Geophys. Res.*, **103**, 1998, pp. 26667-26677.

29. A. Kiraga, Z. Klos, H. Rothkaehl, Z. Zbyszynski, V. N. Oraevsky, et al., "Estimation of Electron Density of Ionospheric Plasma Using Wave, Impedance and Topside Sounder," *Adv. Space Res.*, **20**, 1997, pp. 1083-1095.

30. H. G. James and W. Calvert, "Interference Fringes Detected by OEDIPUS C," *Radio Sci.*, **33**, 1998, pp. 617-629.

31. D. A. Gurnett et al., "The Cassini Radio and Plasma Wave Investigation," *Space Sci. Rev.*, **114**, 2004, pp. 395-463.

32. N. P. Danilkin, "The Results of the Satellite Radio Sounding of the Ionosphere in the Vicinity of the F-Layer Maximum," *Int. J. Geomagn. Aeron.*, **2**, 2001, pp. 173-180.

33. B. W. Reinisch, D. M. Haines, K. Bibl, G. Cheney, I. A. Gulkin, et al., "The Radio Plasma Imager Investigation on the IMAGE Spacecraft," *Space Sci. Rev.*, **91**, 2000, pp. 319-359.

34. J. L. Green and B. W. Reinisch, "An Overview of Results from RPI on IMAGE," *Space Sci. Rev.*, **109**, 2003, pp. 183-210.

35. P. M. E. Decreau, P. Fergeau, V. Krannoselskikh, E. L. Guirriec, M. Leveque, et al., "Early Results from the Whisper Instrument on Cluster: An Overview," *Ann. Geophysicae*, **19**, 2001, pp. 1241-1258.

36. D. A. Gurnett et. al., "Radar Soundings of the Ionosphere of Mars," *Science*, **310**, 2005, pp. 1929-1933.

37. W. L. Flock, *Electromagnetics and the Environment: Remote Sensing and Telecommunications*, Englewood Cliffs, New Jersey, Prentice-Hall, Inc., 1979.

38. J. E. Jackson, "A New Method for Obtaining Electron-Density Profiles from *P'-f* Records," *J. Geophys. Res.*, **61**, 1956, pp. 107-127.

39. J. A. Ratcliffe, *The Magneto-Ionic Theory and Its Applications to the Ionosphere*, New York, Cambridge University Press, 1959.

40. K. G. Budden, *The Propagation of Radio Waves, the Theory of Radio Waves of Low Power in the Ionosphere and Magnetosphere*, New York, Cambridge University Press, 1985.

41. J. M. Kelso, *Radio Ray Propagation in the Ionosphere*, New York, Mcgraw-Hill Electronic Sciences Series, McGraw Hill, 1964.

42. K. Davies, *Ionospheric Radio Propagation,* Washington, National Bureau of Standards Monograph 80, US Government Printing Office, 1965.

43. H. Rishbeth and O. K. Garriot, *Introduction to Ionospheric Physics*, New York, Academic Press, 1969.

44. J. A. Ratcliffe, *An Introduction to the Ionosphere and Magnetosphere*, London, Cambridge University Press, 1972.

45. J. W. Wright and G. H. Smith, "Introductory Paper Review of Current Methods for Obtaining Electron-Density Profiles from Ionograms," *Radio Sci.*, **2**, 1967, pp. 1119-1125.

46. R. D. Hunsucker, *Radio Techniques for Probing the Terrestrial Ionosphere*, (Physics and Chemistry in Space, Volume 22), Berlin, Springer, 1991.

47. B. W. Reinisch, "Modern Ionosondes," in H. Kohl, R. Ruster, and K. Schlegel (eds.), *Modern Ionospheric Science*, Katlenburg-Lindau, Germany, European Geophysical Society, 1996, pp. 440-458.

48. B. W. Reinisch, I. A. Galkin, G. M. Khmyrov, A. V. Kozlov, K. Bibl, et al., "New Digisonde for Research and Monitoring Applications," *Radio Sci.*, **44**, 2009, RS0A24, doi:10.1029/2008RS004115.

49. N. A. Zabotin, J. W. Wright, and G. A. Zhbankov, "NeXtYZ: Three Dimensional Electron Density Inversion for Dynasonde Ionograms," *Radio Sci.*, **41**, 2006, RS6S32, doi:10.1029/2005RS003352.

50. N. A. Zabotin and J. W. Wright, "Principles of Dynasonde Data Acquisition and Processing," XXIX URSI General Assembly, Chicago, 2008, Paper GH11.

51. I. A. Galkin, G. M. Khmyrov, A. V. Kozlov, B. W. Reinisch, X. Huang, et al., "The Artist 5," in P. Song, J. Foster, M. Mendillo, and D. Bilitza, (eds.), *Cp974, Radio Sounding and Plasma Physics*, Lowell, Massachusetts, American Institute of Physics, 2008, pp. 150-159.

52. J. E. Jackson, "Alouette-ISIS Program Summary," NSSDC Report 86-09, National Space Science Data Center, Greenbelt, Maryland, 1986.

53. S. A. Pulinets and R. F. Benson, "Radio-Frequency Sounders in Space," in W. R. Stone (ed.), *Review of Radio Science 1996-1999*, Oxford, Oxford University Press, 1999, pp. 711-733.

54. J. E. Jackson, "Results from Alouette 1, Explorer 20, Alouette 2 and Explorer 31," NSSDC Report 88-10, National Space Science Data Center, Greenbelt, Maryland, 1988.

55. J. E. Jackson and E. S. Warren, "Objectives, History, and Principal Achievments of the Topside Sounder and ISIS Programs," *Proc. IEEE*, **57**, 1969, pp. 861-865.

56. R. F. Benson and D. Bilitza, "New Satellite Mission with Old Data: Rescuing a Unique Data Set," *Radio Sci.*, **44**, 2009, RS0A04, doi:10.1029/2008RS004036.

57. D. L. Carpenter, T. F. Bell, D. Chen, D. Ng, C. Baran, et al., "Proton Cyclotron Echoes and a New Resonance Observed by the Radio Plama Imager Instrument on the IMAGE Satellite," *J. Geophys. Res.*, **112**, 2007, A08208, doi:10.1029/2006JA012139.

58. J. E. Jackson, "Comparisons Between Topside and Ground-Based Soundings," *Proc. IEEE*, **57**, 1969, pp. 976-985.

59. R. F. Benson, P. A. Webb, J. L. Green, D. L. Carpenter, V. S. Sonwalkar, et al., "Active Wave Experiments in Space Plasmas: The Z Mode," in J. W. LaBelle and R. A. Treumann (eds.), *Lect. Notes Phys. 687 Geospace Electromagnetic Waves and Radiation*, New York, Springer, 2006, pp. 3-35.

60. J. E. Jackson, "The Reduction of Topside Ionograms to Electron-Density Profiles," *Proc. IEEE*, **57**, 1969, pp. 960-976.

61. R. F. Benson, "Stimulated Plasma Waves in the Ionosphere," *Radio Sci.*, **12**, 1977, pp. 861-878.

62. E. L. Hagg, E. J. Hewens, and G. L. Nelms, "The Interpretation of Topside Sounder Ionograms," *Proc. IEEE*, **57**, 1969, pp. 949-960.

63. J. E. Titheridge and M. L. Heron, "The Production and Analysis of Transmission Ionograms," *Planet. Space Sci.*, **20**, 1972, pp. 2029-2038.

64. B. D. Muldrew, M. D. Litwack, and P. L. Timleck, "Interpretation of the Statistics of Occurrence of Alouette I Earth Echoes," *Planet. Space Sci.*, **15**, 1967, pp. 611-618.

65. W. M. Farrell, S. M. Clifford, S. M. Milkovich, J. J. Plaut, C. J. Leuschen, et al., "MARSIS Subsurface Radar Investigations of the South Polar Reentrant Chasma Australe," *J. Geophys. Res.*, **113**, 2008, E04002, doi:10.1029/2007JE002974.

66. R. F. Benson, J. L. Green, S. F. Fung, B. W. Reinisch, W. Calvert, et al., "Magnetospheric Radio Sounding on the IMAGE Mission," *Radio Sci. Bull.*, No. 285, 1998, pp. 9-20.

67. R. F. Benson and V. A. Osherovich, "Application of Ionospheric Topside-Sounding Results to Magnetospheric Physics and Astrophysics," *Radio Sci.*, **39**, 2004, RS1S28, doi:10.1029/2002RS002834.

68. R. F. Benson, V. A. Osherovich, J. Fainberg, and B. W. Reinisch, "Classification of IMAGE/RPI-Stimulated Plasma Resonances for the Accurate Determination of Magnetospheric Electron-Density and Magnetic Field Values," *J. Geophys. Res.*, **108**, 2003, 1207, doi:10.1029/2002JA009589.

69. J. L. Donley, L. H. Brace, J. A. Findlay, J. H. Hoffman, and G. L. Wrenn, "Comparison of Results of Explorer XXXI Direct Measurement Probes," *Proc. IEEE*, **57**, 1969, pp. 1078-1084.

70. G. L. Wrenn and P. A. Smith, "Results Derived from Simultaneous Measurements Using the Langmuir Plate and Spherical Ion Probe on Explorer XXXI and the Ionosonde on Alouette II," *Proc. IEEE*, **57**, 1969, pp. 1085-1089.

71. L. H. Brace and J. A. Findlay, "Comparison of Cylindrical Electrostatic Probe Measurements on Alouette II and Explorer XXXI Satellites," *Proc. IEEE*, **57**, 1969, pp. 1057-1060.

72. R. F. Benson, P. A. Webb, J. L. Green, L. Garcia, and B. W. Reinisch, "Magnetospheric Electron Densities Inferred from Upper-Hybrid Band Emissions," *Geophys. Res. Lett.*, **31**, 2004, L20803,doi:1029/2004GL020847.

73. R. F. Benson, "Elusive Upper Hybrid Waves in the Auroral Topside Ionosphere," in R. L. Lysak (ed.), *Auroral Plasma Dynamics, Geophysical Monograph 80*, Washington, DC, American Geophysical Union, 1993, pp. 267-274.

74. J. E. Jackson, "The Analysis of Topside Ionograms," Goddard Space Flight Center Report X-615-67-452, Greenbelt, Maryland, 1967.

75. J. E. Jackson, E. R. Schmerling, and J. H. Whitteker, "Mini-Review on Topside Sounding," *IEEE Trans. Antennas Propagat.*, **AP-28**, 1980, pp. 284-288.

76. G. E. K. Lockwood, "A Modified Iteration Technique for Use in Computing Electron Density Profiles from Topside Ionograms," *Radio Sci.*, **5**, 1970, pp. 575-577.

77. N. P. Danilkin, P. F. Denisenko, and V. V. Sotsky, "Peculiarities of the Inverse Problems of Vertical Radio Sounding of the Ionosphere," *Adv. Space Res.*, **8**, 1988, pp. (4)91-(4)94).

78. J. W. Wright and M. L. V. Pitteway, "Data Acquisition and Analysis for Research Ionograms" in Computer Aided Processing of Ionograms and Ionosonde Records, Rep. UAG-105, Boulder, World Data Center A for Solar Terrestrial Physics, 1998. p. 1-11.

79. B. W. Reinisch and X. Huang, "Automatic Calculation of Electron Density Profiles from Digital Ionograms. 1. Automatic O and X Trace Identification for Topside Ionograms," *Radio Sci.*, **17**, 1982, pp. 421-434.

80. X. Huang and B. W. Reinisch, "Automatic Calculation of Electron Density Profiles from Digital Ionograms 2. True Height Inversion of Topside Ionograms with the Profile-Fitting Method," *Radio Sci.*, **17**, 1982, pp. 837-844.

81. X. Huang, B. W. Reinisch, D. Bilitza, and R. F. Benson, "Electron Density Profiles of the Topside Ionosphere," *Ann. Geophys.*, **45**, 2002, pp. 125-130.

82. D. Bilitza, X. Huang, B. W. Reinisch, R. F. Benson, H. K. Hills, et al., "Topside Ionogram Scaler with True Height Algorithm (TOPIST): Automated Processing of ISIS Topside Ionograms," *Radio Sci.*, **39**, 2004, RS1S27, doi:10.1029/2002RS002840.

83. D. L. Carpenter, T. F. Bell, U. S. Inan, R. F. Benson, V. S. Sonwalkar, et al., "Z-Mode Sounding within Propagation 'Cavities' and Other Inner Magnetospheric Regions by the RPI Instrument on the IMAGE Satellite," *J. Geophys. Res.*, **108**, A12, 2003, 1421, doi:10.1029/2003JA010025.

84. D. A. Gurnett, S. D. Shawhan, and R. R. Shaw, "Auroral Hiss, Z Mode Radiation, and Auroral Kilometric Radiation in the Polar Magnetosphere: DE 1 Observations," *J. Geophys. Res.*, **88**, 1983, pp. 329-340.

85. X. Huang, B. W. Reinisch, P. Song, P. Nsumei, J. L. Green, et al., "Developing an Empirical Density Model of the Plasmasphere Using IMAGE/RPI Observations," *Adv. Space Res.*, **33**, 2004, pp. 829-832.

86. D. B. Muldrew, "Nonvertical Propagation and Delayed-Echo Generation Observed by the Topside Sounders," *Proc. IEEE*, **57**, 1969, pp. 1097-1107.

87. V. S. Sonwalkar, D. L. Carpenter, T. F. Bell, M. A. Spasojevic, U. S. Inan, et al., "Diagnostics of Magnetospheric Electron Density and Irregularities at Altitudes < 5000 km using Whistler and Z Mode Echoes from Radio Sounding on the IMAGE Satellite," *J. Geophys. Res.*, **109**, 2004, A11212, doi:10.1029/2004JA010471.

88. W. Calvert and J. M. Warnock, "Ionosphere Irregularities Observed by Topside Sounders," *Proc. IEEE*, **57**, 1969, pp. 1019-1025.

89. J. H. Whitteker, L. H. Brace, E. J. Maier, J. R. Burrows, W. H. Dodson, et al., "A Snapshot of the Polar Ionosphere," *Planet. Space Sci.*, **24**, 1976, pp. 25-32.

90. F. Daniels, "ISIS-II Spacecraft," CRC Report No. 1218, Ottawa, Communications Research Centre, 1971.

91. W. R. Hoegy and R. F. Benson, "De/ISIS Conjunction Comparisons of High-Latitude Electron Density Features," *J. Geophys. Res.*, **93**, 1988, pp. 5947-5954.

92. R. F. Benson, "Auroral Kilometric Radiation: Wave Modes, Harmonics and Source Region Electron Density Structures," *J. Geophys. Res.*, **90**, 1985, pp. 2753-2784.

93. J. M. Grebowsky, R. F. Benson, P. A. Webb, V. Truhlik, and D. Bilitza, "Altitude Variation of the Plasmapause Signature in the Main Ionospheric Trough," *J. Atmos. Solar-Terr. Phys.*, **71**, 2009, pp. 1669-1676, doi:10.1016/j.jastp.2009.05.016.

94. K. L. Chan and L. Colin, "Global Electron Density Distributions from Topside Soundings," *Proc. IEEE*, **57**, 1969, pp. 990-1004.

95. D. B. Bilitza, B. W. Reinisch, S. M. Radicella, S. Pulinets, T. Gulyaeva, et al., "Improvements of the Internatonal Reference Ionosphere Model for the Topside Electron Density Profile," *Radio Sci.*, **41**, 2006, RS5S15, doi:10.1029/2005RS003370.

96. B. W. Reinisch, P. Nsumei, X. Huang, and D. K. Bilitza, "Modeling the F2 Topside and Plasmasphere for IRI Using IMAGE/RPI, and ISIS Data," *Adv. Space Res.*, **39**, 2007, doi:10.1016/j.asr.2006.05.032.

97. C. Rush, M. Fox, D. Bilitza, K. Davies, L. McNamara, et al., "Ionosphere Mapping: An Update of foF2 Coefficients," *Telecommunication J.*, **56**, 1989, pp. 179-182.

98. S. A. Pulinets, V. P. Kim, V. V. Hegai, V. K. Depuev, and S. M. Radicella, "Unusual Longitude Modification of the Night-Time Midlatitude F2 Region Ionosphere in July 1980 over the Array of Tectonic Faults in the Andes Area: Observations and Interpretation," *Geophys. Res. Lett.*, **25**, 1998, pp. 4133-4136.

99. L. Colin and K. L. Chan, "Model Studies of the Kinked Z Trace in Topside Ionograms," *Proc. IEEE*, **57**, 1969, pp. 1143-1147.

100. J. R. McAfee, "Ray Trajectories in an Anisotropic Plasma near Plasma Resonance," *J. Geophys. Res.*, **73**, 1968, pp. 5577-5583.

101. J. R. McAfee, "Topside Ray Trajectories near the Upper Hybrid Resonance," *J. Geophys. Res.*, **74**, 1969, pp. 6403-6408.

102. D. B. Muldrew, "Electron Resonances Observed with Topside Sounders," *Radio Sci.*, **7**, 1972, pp. 779-789.

103. R. F. Benson, "Plasma Physics Using Space-Borne Radio Sounding," in P. Song, J. Foster, M. Mendillo, and D. Bilitza (eds.), *CP974, Radio Sounding and Plasma Physics*, Lowell, Massachusetts, American Institute of Physics, 2008, pp. 20-33.

104. R. F. Benson and J. Bitoun, "Interpretation of Satellite Gyroharmonic Resonance Observations," *Radio Sci.*, **14**, 1979, pp. 113-123.

105. D. B. Muldrew, "The Poynting Vector Applied to the Complex Refractive Index in a Hot Plasma near the Electron-Cyclotron Frequency, and to the Cyclotron Resonance Observed on Topside Ionograms," *Radio Sci.*, **41**, 2006, RS6006, doi:10.1029/2006RS003496.

106. R. F. Benson, "Ionospheric Plasma Resonances: Time Durations vs. Latitude, Altitude, and fN/fH," *Planet. Space Sci.*, **20**, 1972, pp. 683-706.

107. E. S. Warren and E. L. Hagg, "Observation of Electrostatic Resonances of the Ionospheric Plasma," *Nature*, **220**, 1968, pp. 466-468.

108. H. Oya, "Sequence of Diffuse Plasma Resonances Observed on Alouette 2 Ionograms," *J. Geophys. Res.*, **75**, 1970, pp. 4279-4285.

109. G. L. Nelms and G. E. K. Lockwood, "Early Results from the Topside Sounder in the Alouette II Satellite," in R. L. Smith-Rose (ed.), *Space Research VII*, Amsterdam, North-Holland Publishing Co., 1967, pp. 604-623.

110. D. B. Muldrew, "Electrostatic Resonances Associated with the Maximum Frequencies of Cyclotron-Harmonic Waves," *J. Geophys. Res.*, **77**, 1972, pp. 1794-1801.

111. R. F. Benson, V. A. Osherovich, J. Fainberg, A. F.-Viñas, and D. R. Ruppert, "An Interpretation of Banded Magnetospheric Radio Emissions," *J. Geophys. Res.*, **106**, 2001, pp. 13179-13190.

112. V. A. Osherovich, "Physical Nature of the Diffuse Plasma Resonances in the Ionosphere," *J. Geophys. Res.*, **92**, 1987, pp. 316-320.

113. V. A. Osherovich, R. F. Benson, and J. Fainberg, "Electromagnetic Bounded States and Challenges of Plasma Spectroscopy," *IEEE Trans. Plasma Sci.*, **33**, 2005, pp. 599-608.

114. V. A. Osherovich, "Cylindrical Oscillations of Force-Free Electromagnetic Fields," *Astrophys. Space Sci.*, **121**, 1986, pp. 255-264.

115. V. A. Osherovich, "Cylindrical Oscillations of Force-Free Electromagnetic Fields," *Astrophys. Space Sci.*, **127**, 1986, pp. 185-187.

116. V. A. Osherovich and E. B. Gliner, "Force-Free Electromagnetic Waves," *Solar Physics*, **117**, 1988, pp. 391-397.

117. R. L. Stenzel and J. M. Urrutia, "Force-Free Electromagnetic Pulses in a Laboratory Plasma," *Phys. Rev. Lett.*, **65**, 1990, pp. 2011-2014.

118. H. Oya, "Verification of Theory on Weak Turbulence Relating to the Sequence of Diffuse Plasma Resonances in Space," *Phys. Fluids*, **14**, 1971, pp. 2487-2499.

119. V. A. Osherovich, "The Physical Nature of the Upper Subsidiary Diffuse Resonances," *J. Geophys. Res.*, **94**, 1989, pp. 5530-5532.

120. V. A. Osherovich and R. F. Benson, "The Lower Subsidiary Diffuse Plasma Resonances and the Classification of Radio Emissions Below the Plasma Frequency," *J. Geophys. Res.*, **96**, 1991, pp. 19331-19341.

121. G. Belmont, "Characteristic Frequencies of a Non-Maxwellian Plasma: A Method for Localizing the Exact Frequencies of Magnetospheric Intense Natural Waves near f_{pe}," *Planet. Space Sci.*, **29**, 1981, pp. 1251-1266.

122. J. G. Trotignon, P. M. E. Decreau, J. L. Rauch, O. Randriamboarison, V. Krasnoselskikh, et al., "How to Determine the Thermal Electron Density and the Magnetic Field Strength from the Cluster/Whisper Observations around the Earth," *Ann. Geophysicae*, **19**, 2001, pp. 1711-1720.

123. A. F. Viñas, R. L. Mace, and R. F. Benson, "Dispersion Characteristics for Plasma Resonances of Maxwellian and Kappa Distribution Plasmas and their Comparisons to the IMAGE/RPI Observations," *J. Geophys. Res.*, **110**, 2005, A06202, doi:10.1029/2004JA010967.

124. B. Higel, "Small Scale Structure of Magnetospheric Electron Density through on-Line Tracking of Plasma Resonances," *Space Sci. Rev.*, **22**, 1978, pp. 611-631.

125. R. F. Benson, "Stimulated Plasma Instability and Nonlinear Phenomena in the Ionosphere," *Radio Sci.*, **17**, 1982, pp. 1637-1659.

126. E. L. Hagg and D. B. Muldrew, "A Novel Spike Observed on Alouette II Ionograms," in J. O. Thomas and B. J. Landmark (eds.), *Plasma Waves in Space and Laboratory*, Edinburgh, Edinburgh University Press, 1970, pp. 69-75.

127. H. Oya and R. F. Benson, "A New Method for in Situ Electron Temperature Determinations from Plasma Wave Phenomena," *J. Geophys. Res.*, **77**, 1972, pp. 4272-4276.

128. R. F. Benson, "Ion Effects on Ionospheric Electron Resonance Phenomena," *Radio Sci.*, **10**, 1975, pp. 173-185.

129. R. F. Benson and V. A. Osherovich, "High Order Stimulated Ionospheric Diffuse Plasma Resonances – Significance to Magnetospheric Emissions," *J. Geophys. Res.*, **97**, 1992, pp. 19413-19419.

130. W. Calvert, "Oblique Z-Mode Echoes in the Topside Ionosphere," *J. Geophys. Res.*, **71**, 1966, pp. 5579-5583.

131. R. F. Benson, "An Appreciation of Paul A. Siple," *Eos Trans. AGU*, **75**, 1994, pp. 355 and 361 (also published in *Earth in Space* in September).

132. C. D. Florida "The Development of a Series of Ionospheric Satellites," *Proc. IEEE*, **59**, 1969, pp. 867-875.

133. J. Mar and T. Garrett, "Mechanical Design and Dynamics of the Alouette Spacecraft," *Proc. IEEE*, **59**, 1969, pp. 882-896.

134. C. Franklin, "Alouette/ISIS: How it all Began, Presentation to the IEEE International Milestone in Engineering Ceremony, May 13, 1993, Ottawa," http://ieee.ca/diglib/library/milestone/keynote.htm.

135. C. Franklin, Personal Communication, 2006.

136. J. R. McAfee, "Topside Resonances as Oblique Echoes," *J. Geophys. Res.*, **74**, 1969, pp. 802-808.

137. H. G. James, "Slow Z-Mode Radiation from Sounder-Accelerated Electrons," *J. Atmos. Solar-Terr. Phys.*, **66**, 2004, pp. 1755-1765.

138. H. G. James, "Characteristics of Field-Aligned Density Depletion Irregularities in the Auroral Ionosphere that Duct Z- and X-Mode Waves," *J. Geophys. Res.*, **111**, 2006, A09315, doi:1029/2006JA011652.

139. J. L. Green, "The Struggle to Get RPI on the IMAGE Mission," in P. Song, J. Foster, M. Mendillo, and D. Bilitza (eds.), *CP974, Radio Sounding and Plasma Physics*, Lowell, Massachusetts, American Institute of Physics, 2008, pp. 3-8.

140. W. Calvert, R. F. Benson, D. L. Carpenter, S. F. Fung, D. L. Gallagher, et al., "The Feasibility of Radio Sounding in the Magnetosphere," *Radio Sci.*, **30**, 1995, pp. 1577-1595.

141. D. L. Carpenter, "Highlights of RPI Sounding of the Plasmasphere and Polar Regions at Frequencies in the Whistler and Z-Mode Domains," in P. Song, J. Foster, M. Mendillo, and D. Bilitza (eds.), *CP974, Radio Sounding and Plasma Physics*, Lowell, Massachusetts, American Institute of Physics, 2008, pp. 89-96.

142. S. F. Fung, "Radio Plasma Imager and Measurement of Magnetospheric Field-Aligned Electron Density," in P. Song, J. Foster, M. Mendillo, and D. Bilitza (eds.), *CP974, Radio Sounding and Plasma Physics*, Lowell, Massachusetts, American Institute of Physics, 2008, pp. 97-110.

143. I. A. Galkin, G. M. Khmyrov, A. V. Kozlov, and B. W. Reinisch, "Intelligent Resident Archive for RPI Level 2 Data," in P. Song, J. Foster, M. Mendillo, and D. Bilitza (eds.), *CP974, Radio Sounding and Plasma Physics*, Lowell, Massachusetts, American Institute of Physics, 2008, pp. 111-117.

144. J. DeKeyser, D. L. Carpenter, F. Darrouzet, D. L. Gallagher, and J. Tu, "CLUSTER and IMAGE: New Ways to Study the Earth's Plasmasphere," *Space Sci. Rev.*, **145**, 2009, pp. 7-53, doi:10.1007/s11214-008-9464-7.

145. F. Darrouzet, D. L. Gallagher, N. André, D. L. Carpenter, I. Dandouras, et al., "Plasmaspheric Density Structures and Dynamics: Properties Observed by the CLUSTER and IMAGE Missions," *Space Sci. Rev.*, **145**, 2009, pp. 55-106, doi:10.1007/s11214-008-9438-9.

146. A. Masson, O. Santolík, D. L. Carpenter, F. Darrouzet, P. M. E. Décréau, et al., "Advances in Plasmaspheric Wave Research with CLUSTER and IMAGE Observations," *Space Sci. Rev.*, **145**, 2009, pp. 137-191, doi:10.1007/s11214-009-9508-7.

147. B. W. Reinisch, M. B. Moldwin, R. E. Denton, D. L. Gallagher, H. Matsui, et al., "Augmented Empirical Models of Plasmaspheric Density and Electric Field Using IMAGE and CLUSTER data," *Space Sci. Rev.*, **145**, 2009, pp. 231-261, doi:10.1007/s11214-008-9481-6.

148. P. M. E. Decreau, P. Fergeau, V. Krannoselskikh, M. Leveque, P. Martin, et al., "WHISPER, a Resonance Sounder and Wave Analyser: Performances and Perspectives for the Cluster Mission," *Space Sci. Rev.*, **79**, 1997, pp. 157-193.

149. J. G. Trotignon, J. L. Rauch, P. M. E. Decreau, P. Canu, and J. Lemaire, "Active and Passive Plasma Wave Investigations in the Earth's Environment: The Cluster/ WHISPER Experiment," *Adv. Space Res.*, **31**, 2003, pp. 1449-1454.

150. W. Calvert and J. R. McAfee, "Topside-Sounder Resonances," *Proc. IEEE*, **57**, 1969, pp. 1089-1096.

151. J. R. McAfee, "Electron Plasma Resonances in the Topside Ionosphere," *Fundam. Cosmic Phys.*, **1**, 1974, pp. 71-117.

152. G. E. K. Lockwood, "Excitation of Cyclotron Spikes in the Ionospheric Plasma," *Can. J. Phys.*, **43**, 1965, pp. 291-297.

153. R. F. Benson, "Stimulation of the Harris Instability in the Ionosphere," *Phys. Fluids*, **17**, 1974, pp. 1032-1037.

154. J. Bitoun, L. Fleury, and B. Higel, "Theoretical Study of Gyroresonances with Application to Rocket Experiments," *Radio Sci.*, **10**, 1975, pp. 875-889.

155. R. F. Benson, "An Analysis of Alouette I Plasma Resonance Observations," in J. O. Thomas and B. J. Landmark (eds.), *Plasma Waves in Space and Laboratory*, Edinburgh, Edinburgh University Press, 1970, pp. 25-54.

156. L. Fleury and M. Petit, "Antenna Dependence of Plasma Resonance Patterns," *J. Geophys. Res.*, **79**, 1974, pp. 4817-4820.

157. J. W. King and D. M. Preece, "Observations of Proton Gyro-Effects in the Topside Ionosphere," *J. Atm. and Terr. Phys.*, **29**, 1967, pp. 1387-1390.

158. R. E. Horita, "Proton Cyclotron Frequency Phenomena in the Topside Ionosphere," *Planet. Space Sci.*, **22**, 1974, pp. 793-799.

159. R. E. Horita, "Proton Cyclotron Echoes and Spurs Observed on Alouette II and ISIS II," *Radio Sci.*, **22**, 1987, pp. 671-686.

160. H. Oya, "Generation Mechanism of Proton Cyclotron Echoes Due to Pulsed Radio Frequency Waves in Space Plasma," *J. Geophys. Res.*, **83**, 1978, pp. 1991-2008.

161. G. M. Chen and R. E. Horita, "Proton Cyclotron Echoes at 3fH and 4fH Resonances," *Radio Sci.*, **26**, 1991, pp. 23-29.

162. D. B. Muldrew, "Topside-Sounder Proton-Cyclotron Echo Generation from a Plasma Memory Process and Electron Bernstein-Wave Propagation," *Radio Sci.*, **33**, 1998, pp. 1395-1411.

163. D. B. Muldrew, "Correction To 'Topside-Sounder Proton-Cyclotron Echo Generation from a Plasma Memory Process and Electron Bernstein-Wave Propagation' by D. B. Muldrew," *Radio Sci.*, **35**, 2000, pp. 1047-1048.

164. R. F. Benson, "Evidence for the Stimulation of Field-Aligned Electron Density Irregularities on a Short Time Scale by Ionospheric Topside Sounders," *J. Atm. and Solar-Terr. Phys.*, **59**, 1997, pp. 2281-2293.

165. N. A. Zabotin, D. S. Bratsun, S. A. Pulinets, and R. F. Benson, "Response of Topside Radio Sounding Signals to Small-Scale Field-Aligned Ionospheric Irregularities," *J. Atm. and Solar-Terr. Phys.*, **59**, 1997, pp. 2231-2246.

166. V. A. Osherovich, J. Fainberg, R. F. Benson, and R. G. Stone, "Theoretical Analysis of Resonance Conditions in Magnetized Plasmas When the Plasma/Gyro Frequency Ratio is Close to an Integer," *J. Atm. and Solar-Terr. Phys.*, **59**, 1997, pp. 2361-2366.

167. S. P. Kuo, M. C. Lee, and P. Kossey, "Excitation of Short-Scale Field-Aligned Electron Density Irregularities by Ionospheric Topside Sounders," *J. Geophys. Res.*, **104**, 1999, pp. 19889-19894.

168. R. F. Benson, J. Fainberg, R. A. Hess, V. A. Osherovich, and R. G. Stone, "An Explanation for the Absence of Sounder-Stimulated Gyroharmonic Resonances in the Io Plasma Torus by the Ulysses Relaxation Sounder," *Radio Sci.*, **32**, 1997, pp. 1127-1134.

169. P. Canu, "Observation of Long-Duration Gyroharmonic Resonances: A Refutation of the Short-Duration Explanation for Interpreting the Anomalous URAP Sounder Spectra Observed in the Io Torus," *Radio Sci.*, **36**, 2001, pp. 171-181.

170. R. F. Benson, J. Fainberg, R. A. Hess, V. A. Osherovich, and R. G. Stone, "Comment On 'Observation of Long-Duration Gyroharmonic Resonances: A Refutation of the Short-Duration Explanation for Interpreting the Anomalous URAP Sounder Spectra Observed in the Io Torus' by P. Canu," *Radio Sci.*, **36**, 2001, pp. 1649-1652.

171. P. Canu, "Reply," *Radio Sci.*, **36**, 2001, pp. 1645-1647.

172. D. B. Muldrew, "Radio Propagation Along Magnetic Field-Aligned Sheets of Ionization Observed by the Alouette Topside Sounder," *J. Geophys. Res.*, **68**, 1963, pp. 5355-5370.

173. R. A. Helliwell, *Whistlers and Related Ionospheric Phenomena*, Stanford, California, Stanford University Press, 1965.

174. W. Calvert, "Wave Ducting in Different Wave Modes," *J. Geophys. Res.*, **100**, 1995, pp. 17491-17497.

175. D. L. Carpenter, M. A. Spasojevic, T. F. Bell, U. S. Inan, B. W. Reinisch, et al., "Small-Scale Field-Aligned Plasmaspheric Density Structures Inferred from RPI on IMAGE," *J. Geophys. Res.*, **107**, A9**,** 2002, 1258, doi:10.1029/2001JA009199.

176. S. F. Fung, R. F. Benson, D. L. Carpenter, J. L. Green, V. Jayanti, et al., "Guided Echoes in the Magnetosphere: Observations by Radio Plasma Imager on IMAGE," *Geophys. Res. Lett.*, **30**, 11, 2003, 1589, doi:10.1029/2002GL016531.

177. P. L. Dyson and R. F. Benson, "Topside Sounder Observations of Equatorial Bubbles," *Geophys. Res. Lett.*, **5**, 1978, pp. 795-798.

178. R. F. Benson, "Field-Aligned Electron Density Irregularities Near 500 km – Equator to Polar Cap Topside Sounder Z Mode Observations," *Radio Sci.*, **20**, 1985, pp. 477-485.

179. B. W. Reinisch, X. Huang, P. Song, G. S. Sales, S. F. Fung, et al., "Plasma Density Distribution Along the Magnetospheric Field: RPI Observations from IMAGE," *Geophys. Res. Lett.*, **28**, 2001, pp. 4521-4524.

180. D. B. Muldrew, "Characteristics of the Coupled Z Mode at Arecibo," *Radio Sci.*, **28**, 1993, pp. 379-388.

181. D. B. Muldrew, "Correction To 'Characteristics of the Coupled Z Mode at Arecibo' by D. B. Muldrew," *Radio Sci.*, **29**, 1994, pp. 673-674.

182. B. W. Reinisch, X. Huang, P. Song, J. L. Green, S. F. Fung, et al., "Plasmaspheric Mass Loss and Refilling as a Result of a Magnetic Storm," *J. Geophys. Res.*, **109,** 2004, A01202, doi:10.1029/2003JA009948.